Astron. Astrophys. 128, 212–229 (1983)

ASTRONOMY AND ASTROPHYSICS

Interstellar radiation field and dust temperatures in the diffuse interstellar matter and in giant molecular clouds

J. S. Mathis[1], P. G. Mezger[2], and N. Panagia[3]

[1] Washburn Observatory, University of Wisconsin-Madison, 475 N. Charter St., Madison, WI 53706, USA
[2] Max-Planck-Institut für Radioastronomie, Auf dem Hügel 69, D-5300 Bonn 1, Federal Republic of Germany
[3] Istituto di Radioastronomia, Via Irnerio 46, I-40126 Bologna, Italy

Received February 21, accepted June 29, 1983

Summary. In Paper I (Mezger et al., 1982) we have investigated the emission spectrum of dust in both the diffuse interstellar matter (ISM) and in Giant Molecular Clouds (GMC's). This included an estimation of dust absorption cross sections from the Lyman continuum to the submm range and a redetermination of the interstellar radiation field (ISRF) using the most recent observations. In this paper we reevaluate the ISRF as a function of galactocentric distance D_G, taking into account the results of recent surveys of the galactic 2.4 μm and 3.4 μm emission as well as of FIR surveys of the galactic plane as discussed in Paper I, and using an improved model of the variation of dust opacity in the galactic plane. We then determine the radiation field inside GMC's, including the radiation from the GMC itself, as a function of both D_G and the extinction A_V measured from the surface of the cloud. Next, we calculate the dust temperatures of the MRN composite graphite/silicate dust model (Mathis et al., 1977) in the radiation field within the cloud. The main results are: (i) The ISRF between 0.09 and 8 μm is dominated by stellar radiation and between 8 and 1000 μm is dominated by reemitted radiation from dust grains. The total energy density of the ISRF between $D_G = 10$ and 5 kpc increases by a factor seven. The ISRF attains its intensity maximum at ~ 1 μm. (ii) The dominant sources of heating in GMC's are stellar radiation for graphite grains and FIR heating for silicate grains. The contribution of normal field stars embedded in GMC's to the heating of dust is normally negligible. This may be different in a cloud which contains many low-mass pre-MS stars. While the temperatures of graphite grains in the diffuse ISM and in the outer sheaths of GMC's are twice as high as the temperatures of silicate grains, both types of grains attain approximately equal temperatures between 5 and 7 K deep inside GMC's. (iii) The stellar radiation absorbed in the outer layers of GMC's is practically all converted into FIR radiation whose integrated mean intensity is about five times that of the diffuse galactic FIR emission.

Key words: dust – interstellar matter – interstellar radiation field

1. Introduction

In a recent paper (Mezger et al., 1982, hereafter referred to as Paper I) we have tried to explain the origin of the diffuse galactic FIR/submm emission. We found that: (i) The observed dust extinction cross-sections between the Lyman continuum (Lyc) and 1 mm can be reasonably reproduced by the MRN (Mathis et al., 1977) dust model, which consists of a mixture of graphite (Gr) and silicate (Si) grains with a size distribution $f(a) \propto a^{-3.5}$. (ii) The diffuse emission at wavelengths $\gtrsim 20$ μm can be explained by contributions from dust heated by O stars to temperatures of $T_{gr} \sim 40$ K and $T_{si} \sim 30$ K, respectively ($\sim 80\%$); and dust associated with the diffuse atomic intercloud gas which is heated by the the general interstellar radiation field (ISRF) to temperatures of $T_{gr} \sim 19$ K and $T_{si} \sim 10$ K, respectively ($\sim 20\%$). (iii) The mean intensity of the ISRF is practically independent of the distance from the galactic center. (iv) The contribution from dust associated with quiescent molecular clouds (i.e. clouds containing no luminous sources of heating such as OB stars) to the total diffuse FIR/submm emission is small ($\lesssim 7\%$).

Nevertheless the temperature of dust inside quiescent molecular clouds is of great interest for both their energy balance and for the possibility of detecting density structures of these clouds through observations of the thermal radiation of dust. Furthermore, the overwhelming fraction of molecular hydrogen appears to be contained in quiescent clouds rather than in clouds with very young OB stars embedded (see Sect. 5.2). In Sect. 2 of this paper we reinvestigate the intensity of the ISRF in the vicinity of the sun and its variation with galactocentric distance, D_G, taking into account the latest observational data and their interpretation. It is found that we have strongly overestimated the variation of dust opacity with D_G and that we have neglected the contribution from M-type giants, whose presence is revealed through observations of the unexpectedly strong 2.4 μm and 3.4 μm emission from the galactic plane. Taking these effects into account, an increase of the integrated mean intensity of the ISRF between $D_G = 10$ and 5 kpc by a factor of ~ 7 is found. Furthermore, we have included in our considerations the presence of diffuse galactic FIR emission between 8 and 1000 μm from circumstellar and interstellar dust.

In Sect. 3 of this paper we recompute the temperature of dust grains in the diffuse interstellar matter (ISM) which is now found to vary for graphite grains from 25.4 K at the galactocentric distance $D_G = 5$ kpc to 16.6 K at 13 kpc, and for silicate grains from 12.8 K at 5 kpc to 8.9 K at 13 kpc. It is also found (Sect. 5) that radiation from grains associated with diffuse atomic gas and heated by the general ISRF may contribute $\sim 40\%$ to the diffuse galactic FIR/submm emission rather than $\sim 20\%$ as found in Paper I.

In Sect. 4 of this paper we compute the radiation field inside Giant Molecular Clouds (GMC's), taking into account direct stellar radiation and FIR reemission from dust grains, and we

Send offprint requests to: P. G. Mezger

compute and compare heating rates for dust grains made of graphite and silicates. FIR heating becomes important for silicate grains for visual extinctions $A_V \gtrsim 2$ mag from the surface of the cloud, while this happens for graphite grains only deep inside very opaque clouds, for $A_V \gtrsim 40$ mag. Minimum dust temperatures maintained by FIR heating at the center of very opaque dust clouds are in the range from 5–5.5 K at $D_G = 10$ kpc, and 7–8 K at $D_G = 5$ kpc. The contribution of quiescent GMC's to the diffuse galactic FIR/submm emission is only $\sim 2\%$ of the emission from dust associated with the diffuse ISM (Sect. 5).

We discuss in Sect. V.1 the nature of the stellar components, in Sect. V.2 the origin of the diffuse galactic FIR/submm emission, in Sect. V.3 the FIR field near and inside GMC's and in Sect. V.4 the possibility to detect protostars in their earliest evolutionary stages.

In this paper we discuss mean radiation intensities, J_λ, and fluxes, F_λ. When we present the results graphically, J_λ and F_λ are multiplied by the wavelength λ. In this way, since $\int_{\lambda_1}^{\lambda_2} J_\lambda d\lambda = \int_{\ln\lambda_1}^{\ln\lambda_2} J_\lambda d\ln\lambda$, intensities in different logarithmic intervals can be directly compared.

2. The interstellar radiation field (ISRF)

The mean intensity of radiation at a typical point in the Galaxy can be usefully thought of as being divisible into two distinct wavelength ranges. The ultraviolet-visible-near infrared region of the spectrum ($\lambda \leqq 8$ μm) is produced practically entirely from stars of various sorts. The middle- and far-infrared region ($\lambda \gtrsim 8$ μm) is produced entirely from dust, either warm (in circumstellar shells) or cold. We discuss each of these spectral regions in turn.

2.1. The stellar radiation field

Our approach to determining the ISRF at all values of D_G is to fit the well-observed spectrum of the ISRF in the solar vicinity (assumed to be at $D_G = 10$ kpc) with a suitable mixture of four components of stars of various temperatures. We then determine the variation of each component with D_G by analogy with other galaxies or by observations of certain spectral characteristics in our Galaxy. In Paper I, Appendix A, the ISRF in the solar vicinity was described by a UV component which we label component 1 and two diluted blackbody radiation fields with $T_2 = 7500$ K, dilution factor $W_2 = 10^{-14}$ and $T_3 = 4000$ K, $W_3 = 1.65\,10^{-13}$. In our reevaluation of the ISRF in Appendix A of this paper it is shown that a fourth component with $T_4 = 3000$ K and $W_4 = 4.0\,10^{-13}$ has to be added to account for the NIR emission from the galactic plane as observed by various Japanese groups (see the review paper by Okuda, 1981 and references therein) but that the dilution factor of the third stellar component has to be decreased to $W_3 = 1.00\,10^{-13}$. This changes the ISRF as given in Appendix C of Paper I appreciably only for wavelengths $\lambda > 1$ μm. For $\lambda \gtrsim 2.4$ μm the average intensity of the ISRF is increased by a factor ~ 1.5. The integrated intensity is

$$\int_{0.09}^{8\,\mu m} 4\pi J_\lambda^{\odot} d\lambda = 2.17\,10^{-2}\ \mathrm{erg\,cm^{-2}\,s^{-1}},$$

which is 28% higher than the corresponding value given in Paper I. It corresponds to the radiation intensity of a blackbody at $T = 3.14$ K. This value is now in excellent agreement with the average of 17 measurements of Keene (1981), who determined the mean intensity of the ISRF from the integrated FIR/submm flux

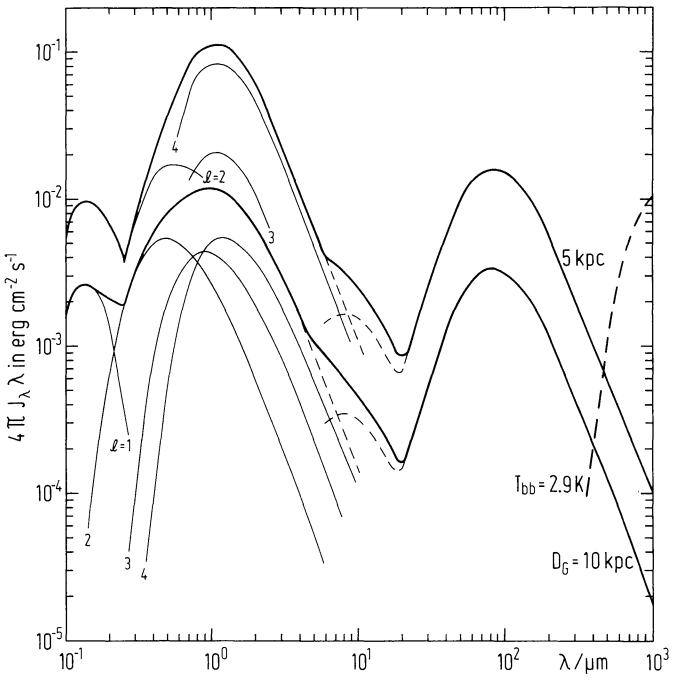

Fig. 1. The interstellar radiation field (ISRF) at galactocentric distances $D_G = 5$ and 10 kpc, respectively. Curves labelled $\ell = 1$, 2, 3, 4 relate to the contributions of the four stellar components to the ISRF. For wavelengths $\gtrsim 8$ μm the ISRF is dominated by reemission from dust grains

density from 9 globules to be $(2.1^{+1.2}_{-0.8})\ 10^{-2}\ \mathrm{erg\,cm^{-2}\,s^{-1}}$. The wavelength times the mean intensity of the ISRF in the solar vicinity, $4\pi\lambda J_\lambda(D_G = 10\ \mathrm{kpc})$, is shown in Fig. 1, together with the contributions of the four stellar components.

In Paper I, to compute the variation of the intensity of the ISRF with galactocentric distance D_G, we adopted an exponential variation of the volume emissivity of the stellar components 1, 2, and 3, $j_\ell = J_\ell(0)\exp\{-\alpha_\ell D_G\}$, with $\alpha_1 = \alpha_2 = \alpha_3 = 0.23\ \mathrm{kpc}^{-1}$. We also assumed the dust opacity is $k = k(0)\exp\{-\beta D_G\}$ with $\beta = 0.43\ \mathrm{kpc}^{-1}$. This steep increase of the dust opacity with D_G resulted from an increase of the mean gas density, both atomic and molecular hydrogen, $\propto \exp\{-0.23(D_G - D_\odot)\}$, and of the dust-to-gas mass ratio $m_d/m_g \propto Z \propto \exp\{-0.20(D_G - D_\odot)\}$, with Z the heavy element abundance. However, Güsten (1981) pointed out that for wavelengths at which dust in both the diffuse ISM (i.e., H I regions) and molecular clouds contribute to the average opacity in the Galaxy, the relation

$$k_V(D_G) = 1.875 n_{\mathrm{HI}}(D_G)\frac{Z(D_G)}{Z_\odot} + 0.11\varepsilon(^{12}\mathrm{CO})\ \mathrm{mag\,kpc}^{-1} \qquad (1)$$

between the visual extinction in magnitudes per kpc, mean density of atomic hydrogen n_{HI} in cm^{-3} and ^{12}CO emissivity in K km s^{-1} kpc^{-1} should be used. This relation assumes that the dust-to-gas mass ratio $m_d/m_g \propto n(^{12}\mathrm{CO})/n(\mathrm{H}_2)$. Güsten's evaluation of $k_V(D_G)$ can be approximated by an exponential function [Eq. (A 5a)] with $\beta = 0.26$ for $D_G \geqq 4$ kpc; and by a linear decrease from $k_V(4\ \mathrm{kpc}) = 3.00\ \mathrm{mag\,kpc}^{-1}$ to $0\ \mathrm{mag\,kpc}^{-1}$ at about the galactic center. The corresponding visual extinction in the plane is 19.5 mag between $D_G = 10$ kpc and $D_G = 4$ kpc and 6 mag from

4– ~0 kpc. (We neglect the inner 0.3 kpc in our model because of the very special nature of the central region.) Appendix C discusses both the opacity as function of wavelength and as function of galactocentric distance. It is shown there that one actually should use a frequency dependent β which varies from ~0.12 at UV and optical wavelengths to 0.26 at NIR and longer wavelengths to take the clumping of dust in GMC's approximately into account. Our model computations show, however, that the ISRF at short wavelengths is rather insensitive to β so that our model with $\beta=\text{const}=0.26$ yields reasonable results throughout the entire wavelength range from 0.09–1000 μm.

We approximate the volume emissivity of each stellar component, $j_\ell(D_G)$, by exponentials [Eq. (A5b)] with an inner cut-off:

$$j_\ell(D_G)=j_0\exp\{-\alpha_\ell D_G\}; \quad (D_G>D_{\min,l})$$
$$=0 \quad (D_G<D_{\min,l}).$$

Values of the gradients α_ℓ used in this paper are compiled in Table A1 together with the corresponding values $D_{\min,l}$. The choice of these parameters is explained in the footnotes of Table A1. Volume emissivities relating to the four stellar components are compiled in Table A2. They are obtained by forcing the model to yield the solar ISRF; i.e. by solving Eq. (A7a) for $4\pi J_\lambda(D_G=10\,\text{kpc})=4\pi J_\lambda^\odot$, the average intensity of the ISRF in the solar vicinity as derived from observations in Appendix A and shown in Fig. 1 for $D_G=10$ kpc, substituting for I_c and I_{ac} Eqs. [(A8a) and (A8b)], respectively.

We now explain the choice of the parameters for the stellar components 3 and 4 in more detail. Both Maihara et al. (1978) and Hayakawa et al. (1977, 1978) found that the observed ridge line intensity at $\lambda=2.4$ μm [i.e. $I_{2.4}^\odot(l,b=0°)$] at galactic longitudes $l\lesssim 60°$ does not follow the galactic mass distribution. The observed 2.4 μm radiation is very narrow in b, and implies sources which have a scale height of only about 50 pc. The 2.4 μm radiation is also strongly concentrated towards the inner $l\leqq 30°$, so that the intensity towards the galactic center is about 15–20 times that towards the anticenter. Component 4 is a very luminous component of the Galaxy and we emphasize that it is required by observations and is not an artifact of our model. To reproduce the observed ridge line intensity of the diffuse galactic 2.4 μm emission the stars which account for component 4 must be distributed in a ring between galactocentric distances of 4 and 8 kpc. These stars appear to be primarily M giants although M supergiants also have the required distribution (Kawara et al., 1982). To model these sources, we use a new component 4, with a Planck spectrum with $T=3000$ K, diluted by a factor $W_4=4.0$ E-13, and scale height $H_4=50$ pc, whose emissivity is steeply increasing towards the center of the Galaxy. For $l\gtrsim 60°$, on the other hand, the observed ridge line intensity can be explained by M-giants with a density as observed in the solar vicinity, which scales with the mass distribution (Hayakawa et al., 1979). To fit the observed ridge line variation at 2.4 μm we choose a value of the gradient of component 4, $\alpha_4=0.75$, which makes its contribution in the anticenter direction negligible at $D_G=10$ kpc.

If we try to fit the observed longitude distribution of the intensity at 2.4 μm as given by Eq. (A3) by simply adding to the ISRF as given in Appendix C of Paper I a diluted blackbody radiation of 3000 K, we obtain values which are too high for both the mean radiation intensity in the solar vicinity for $\lambda>1$ μm and for the ridge line intensities in the center and anticenter directions, respectively. We therefore decreased the contribution of component 3 by a factor 0.61. This four-component model of the stellar distribution in the galactic disk not only yields a good approximation of the average radiation density in the solar vicinity, but also approximates the ridge line intensity at 2.4 μm, as given by Hayakawa et al. (1978, 1979) outside the galactic center region, very well. It should be mentioned that the latest results by Hayakawa et al. (1981), which were not considered in our model fit, suggest a somewhat lower ridge line intensity. (See also the discussion at the end of Appendix A.)

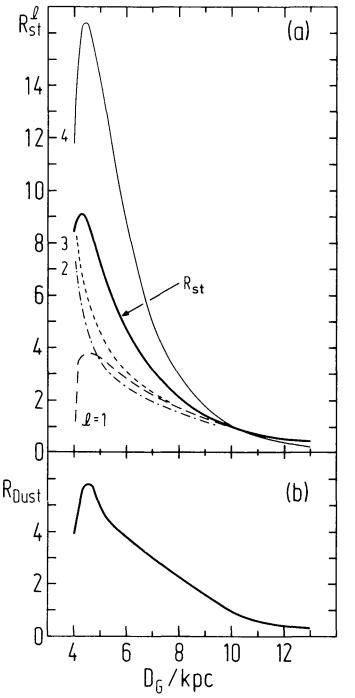

Fig. 2. a Integrated intensities of the four stellar components as a function of the galactocentric distance D_G, relative to the corresponding integrated intensities at $D_G=10$ kpc. R_{st} refers to the total integrated spectrum between 0.09 and 8 μm. **b** The corresponding variation of the intensity of the ISRF between 8 and 1000 μm which is dominated by the reemission from dust grains

The mean intensity of the ISRF is then obtained by adding up the contributions of the four components as given by Eq. (A7a)

$$4\pi J_\lambda(D_G)=\sum_{\ell=1}^{4}4\pi J_\lambda^\ell(D_G)=F\{\tau_\lambda(D_G)\}\sum_{i=1}^{4}\phi_\lambda^\ell(D_G), \tag{2}$$

where $F(\tau)$ and ϕ_λ^ℓ are functions defined in Appendix A.

The spectral distribution of the ISRF is given for some selected values of D_G in Table A3. The quantity $4\pi J_\lambda(D_G)\lambda=\sum_l 4\pi J_\lambda^\ell(D_G)\lambda$ is shown in Fig. 1 for $D_G=5$ and 10 kpc. One recognizes how the relative contributions of the individual components and hence the spectral shape of the total ISRF between 0.1 and 8 μm change, both as result of the increase of the dust opacity towards the galactic center and of the different gradients of the volume emissivities of the four stellar components.

In Fig. 2a are shown as a function of D_G the integrated average intensities of the ISRF of the four stellar components, relative to the corresponding intensities at $D_G=10$ kpc.

$$R_{st}^\ell(D_G)=\int_{0.09}^{8\,\mu\text{m}}4\pi J_\lambda^\ell(D_G)d\lambda\Big/\int_{0.09}^{8\,\mu\text{m}}4\pi J_\lambda^\ell(D_\odot)d\lambda \tag{3a}$$

and of the total ISRF

$$R_{st}(D_G)=\sum_{\ell=1}^{4}\int_{0.09}^{8\,\mu m}4\pi J_\lambda^\ell(D_G)d\lambda\Big/\sum_{\ell=1}^{4}\int_{0.09}^{8\,\mu m}4\pi J_\lambda^\ell(D_\odot)d\lambda. \quad (3b)$$

The relation

$$4\pi J_\lambda(D_G)\simeq\sum_{l=1}^{4}4\pi J_\lambda^\ell(D_\odot)R_{st}^\ell(D_G) \quad (4)$$

is a good approximation of Eq. (2).

The rapid change of components 1 and 3 in Fig. 2a between 4 and 5 kpc is an artifact of our model's abruptly cutting off their emissivity at 4 kpc. It furthermore is very sensitive to the dust distribution within the inner 4 kpc which is very poorly known. In reality, a more continuous change of both dust and stellar emission is required. We will emphasize therefore only results for $D_G \geqq 5$ kpc.

2.2. *The diffuse galactic* FIR *emission from dust grains*

As estimated in Paper I, about one quarter of the total stellar emission in our Galaxy is absorbed by dust grains and reemitted in the FIR. The mean intensity of the diffuse FIR emission in the solar vicinity is shown in Fig. 1. The spectral distribution is that shown in Paper I, Fig. 1. The integration over solid angle is performed in Appendix B of this paper. The reemission from dust dominates the ISRF for wavelengths $\gtrsim 8\,\mu m$. The integrated intensity is

$$\int_{8}^{1000\,\mu m}4\pi J_\lambda^\odot d\lambda = 4.94\,10^{-3}\,\mathrm{erg\,cm^{-2}\,s^{-1}} \quad (5)$$

which is 18% of the ISRF integrated from 0.09 to 1000 μm. To compute the D_G-dependence of the intensity of the ISRF at wavelengths $\geqq 8\,\mu m$ we neglect dust opacity, and use the volume emissivity derived by Boissé et al. (1981) as described in Appendix B. The quantity

$$R_{\mathrm{Dust}}(D_G)=\int_{8}^{1000\,\mu m}4\pi J_\lambda(D_G)d\lambda\Big/\int_{8}^{1000\,\mu m}4\pi J_\lambda^\odot d\lambda \quad (6)$$

is shown in Fig. 2b. Since we assume the FIR spectrum to be independent of D_G [in fact, as shown in Fig. 8 of Mezger (1983), the emission of dust associated with both diffuse atomic gas and ELD H II regions, which are the principal contributors to the diffuse galactic FIR field, has nearly the same radial dependence], we have

$$4\pi J_\lambda(D_G)=R_{\mathrm{Dust}}(D_G)4\pi J_\lambda^\odot$$

which is identical with Eq. (B3). The ISRF at $D_G=10$ kpc between 8 and 1000 μm is compiled in Table B1 and shown in Fig. 1. Between 4 and 80 μm the ISRF is highly uncertain and should be considered as a first, rough approximation until better observational data are available. Also note that the ISRF as compiled in Tables A3 and B1, respectively does not join smoothly near $\lambda=10\,\mu m$, as indicated by the dashed curves in Fig. 1. However, the ISRF is low in this spectral region, and our results are not influenced by how we join the visual and FIR peak intensities.

3. Dust temperatures in the diffuse Interstellar Medium (ISM)

The formulae for computing dust temperatures (Sect. III of Paper I or Sect. 4.4 of this paper) have been reevaluated using the cross sections given in Table C1 of this paper (which are essentially those used in Paper I) and the radiation field derived in Sect. 2 of this paper (which is significantly different from that in Paper I). The result is shown as function of the galactocentric distance D_G in Fig. 3.

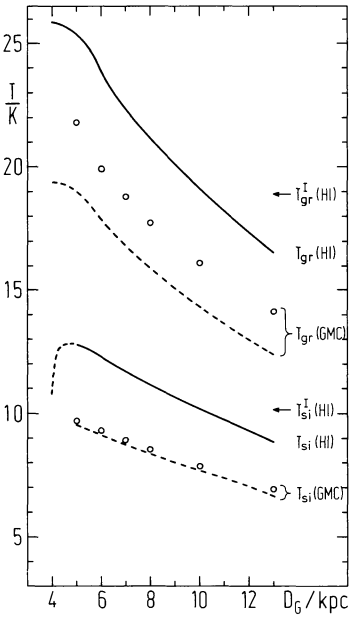

Fig. 3. Temperatures of graphite (gr) and silicate (si) grains heated by the ISRF, shown here as a function of galactocentric distance D_G. (H I) refers to grains associated with diffuse ISM (atomic hydrogen), (GMC) refers to dust associated with giant molecular clouds. Open circles refer to temperatures obtained by fitting Planck functions to computed cloud spectra, such as shown in Fig. 7a and b. Dashed curves refer to the simple approximation $T(\mathrm{GMC})\sim(0.5e^{-1})^{1/6}T(\mathrm{H\,I})=0.75T(\mathrm{H\,I})$. T^{I} are temperatures derived in Paper I

In Fig. 3, $T_i^{\mathrm{I}}(\mathrm{H\,I})$ and arrows relate to the corresponding dust temperatures in Paper I, which were derived for the ISRF in the solar vicinity and thought to be independent of D_G. The fact that those temperatures are slightly lower than the temperatures derived here for the solar vicinity ($D_G=10$ kpc) is due to the increase of the integrated ISRF by 28% relative to the corresponding value derived in Paper I. Silicate grains absorb primarily in the far UV. Their temperature, $T_{\mathrm{si}}(D_G)$, is therefore correlated with the integrated radiation intensity of stellar component 1, whose variation with D_G is shown as Curve 1 in Fig. 2a. Graphite grains, on the other hand, absorb most of the radiation in the visual and near IR, so that $T_{\mathrm{gr}}(D_G)$ is dominated by the variations with D_G of the integrated intensities of stellar components 2, 3, and 4, which are shown as curves 2, 3, and 4 in Fig. 2a.

4. Dust temperatures of Giant Molecular Clouds (GMC)

Solomon et al. (1978) have reviewed the characteristics of GMC's in the Galaxy. As average parameters they derive: linear size ~ 40 pc, gas temperature $T_k\sim 10$ K, $n_{\mathrm{H_2}}\sim 300\,\mathrm{cm^{-3}}$, and $M_{\mathrm{H_2}}\sim 5\,10^5\,M_\odot$. Their estimated total number of GMC's between galactocentric distances 4 and 8 kpc is ~ 4000, yielding a total mass of molecular hydrogen of at least $2\,10^9\,M_\odot$. Güsten (1981)

reevaluated earlier CO surveys, taking into account some numerical errors and a variation of the heavy element abundance with D_G. He arrived at a considerably lower mass of molecular hydrogen, $M_{H_2} \sim 6\,10^8\,M_\odot$ between 2 and 13 kpc, which is about half of the total mass of atomic hydrogen contained in this region of the Galaxy, and about 1/3 of the total mass of molecular hydrogen as estimated by Solomon et al. (1978). We therefore consider the above given average parameters of GMC's rather as upper limits to real GMC's. The visual extinction of such a "standard" cloud from its center to the surface is ~ 20 mag. Of course, there may be condensations in GMC's where the extinction is considerably higher.

In Paper I we treated the radiation from dust associated with quiescent clouds (i.e. GMC's which are not internally heated by OB stars or supergiants) rather summarily, by assuming that their spectrum can be described by graphite and silicate grains whose temperatures are reduced by a factor $(0.5\ e^{-1})^{1/(4+m)} \sim 0.75$ relative to the corresponding grain temperatures derived for the diffuse ISM. It is the main aim of this paper to predict the dust temperature at each point inside a GMC. This temperature – as in the case of the diffuse ISM – is practically completely determined by the balance of radiation absorbed and emitted by the dust, independently of whether or not the gas is dense enough ($n_{H_2} \gtrsim 10^4\ cm^{-3}$) to be thermally coupled to the gas. Compared to the cooling rate of dust grains the cooling rate of gas due to line emission is always only a few percent. Therefore, whenever the gas is thermally coupled to dust it will approach the dust temperature. Under normal circumstances the gas will never affect the dust temperatures. The main sources of radiative heating of the dust inside GMC's, in the following labelled by the subscript j, are:

1. The stellar radiation between 0.09 and 8 μm as derived in Sect. 2.1, but heavily modified by absorption and scattering.
2. The diffuse galactic FIR radiation emitted primarily by dust which is heated by OB stars (Sect. 2.2).
3. The FIR radiation field of the cloud itself, arising primarily from the sheath of warm grains on the cloud's surface.
4. Field stars which happen to be embedded within the GMC.

Werner and Salpeter (1970) first treated grain temperatures in GMC's, taking into account the heating sources 1 and 3 (which are, in fact, in most cases the dominant heating sources). However, with the ISRF and the absorption cross-sections of dust derived in this paper, our results are quantitatively quite different from those derived by Werner and Salpeter.

4.1. *Radiative transfer in a dusty* GMC

Let us consider a spherical GMC which has a visual extinction A_{V0} from the center to the surface of the cloud, and which has an isotropic radiation intensity, $I_{\lambda 0}$, incident upon the surface. In this paper, we assume the GMC is uniform throughout. In this case, we can use the exact numerical solution of Flannery et al. (1980) to determine the mean intensity of radiation within the cloud.

We fitted the numerical solution by a scheme suggested by the very simple two-stream treatment of radiation transfer of Code (1973). This scheme can be applied to either a sphere or to a plane of extinction optical depth $\tau_0 = A(\lambda)/1.086$, if $A(\lambda)$ is, as usual, expressed in magnitudes. Code's work suggests that J, the mean intensity at optical depth τ from the center of the cloud or slab with an isotropic intensity I_0 incident upon it, can be written in the form

$$J(\tau) = \frac{I_0[\exp(Q\tau) + \exp(-Q\tau)]}{(1+U)\exp(Q\tau_0) + (1-U)\exp(-Q\tau_0)}, \tag{8}$$

where

$$Q \equiv [(1-a)(1-ag)]^{1/2}\bar{\mu}^{-1}, \tag{8a}$$

$$U \equiv [(1-a)/(1-ag)]^{1/2} \tag{8b}$$

with a = albedo of the grains at the wavelength in question, $g = \langle\cos\theta\rangle$ = mean cosine of the angle of scattering at that wavelength, and $\bar{\mu}$ is a parameter related to the geometry (being smaller for spheres), but involving a and g as well. It can be regarded as the "best" value of the cosine of the ray in the two-stream approximation. Code (1973) found that expressions of the above form give an excellent fit to the flux emerging from a spherical dust cloud surrounding a central point source. We fitted the expressions (8) to the exact solutions of $J(\tau)$ of Flannery et al. (1980), using a least-squares technique to pick the best form for $(\bar{\mu})^{-1}$ which is linear in τ, g, and a. We found that

$$\bar{\mu}^{-1} = 1.135 + 0.425\tau/\tau_0 + 0.2775(a-0.4) - 0.105(g-0.25) \tag{8c}$$

gives a good fit to the exact solution, with the average deviation for (J/I_0) differing by only 6% from the exact solutions for $\tau_0 = 5$, 10, 15, and 20. At the center of the cloud with $\tau_0 = 20$ the expressions (8) give a radiation field too low by up to 50% for $a = 0.4$, $g = 0.5$, but the field has dropped by a factor of 10^7 and is negligible anyway. We checked the consistency of Eq. (8) by calculating the radiative flux into the cloud with that emerging from the cloud. For $5 \lesssim \tau_0 \lesssim 20$, the result was satisfactory (about a 10% difference). For $\tau_0 = 184$, corresponding to $A_V = 200$, about 1.5 times as much flux emerged as entered. We corrected the emergent flux and the internal radiation field by this factor.

Flannery et al. (1980) do not give solutions for clouds optically thicker than $\tau_0 = 20$, but we use the expressions (8) and (9) for even larger values of τ_0 because we feel that the error in grain temperatures introduced by the use of these expressions in place of exact radiation transfer calculations is small in comparison to the uncertainties in the optical properties of the grains, discussed below.

With the ISRF used to give I_0, the intensity incident upon the cloud surface, Eq. (8) predicts the radiation field at a point which has a visual extinction of A_V magnitudes from the surface of the cloud. From this field, we compute $T_{gr}(A_V)$, the average graphite grain temperature, by balancing the rates of absorption and emission of energy from the graphite. Similarly, we find the silicate temperature $T_{si}(A_V)$. We next calculate the FIR radiation field arising from the radiation of the grains within the cloud $I_{\lambda,cl}$ by solving the equation of transfer

$$\frac{dI_{\lambda,cl}}{d\tau_V} = -\frac{\sigma_\lambda}{\sigma_V} I_{\lambda,cl} + \sum_i \frac{B_\lambda(T_i)\sigma_{\lambda,i}}{\sigma_V}, \tag{9}$$

where $I_{\lambda,cl}$ is the intensity of the FIR from the cloud itself, τ_V = optical depth at 0.55 μm along the path, and the subscript i refers to graphite and silicates.

We solved Eq. (9) for, typically, eight directions at a point in the outer layers of the cloud by directly integrating along the path in each direction, after changing variables to temperature instead of τ_V. From the values of I_λ calculated in the various directions the quantity $4\pi J_{\lambda,cl} = 2\pi \int I_{\lambda,cl} \sin\theta\, d\theta$ as determined by direct integration. This radiation field is then added to that produced directly by the attenuated ISRF and that produced by embedded field stars. The addition of the cloud's radiation field increases the grain temperatures used in Eq. (9) to compute the cloud's field, so iterations are required. Thus, our procedure was to: (a) calculate $4\pi J_\lambda$ from the ISRF [Eq. (8)] and embedded field stars; (b)

calculate dust temperatures (and, therefore, emissivities) from that field; (c) calculate $I_{\lambda,\mathrm{cl}}$ from Eq. (9) and then $4\pi J_{\lambda,\mathrm{cl}}$ by integrating over solid angles; (d) add the values of $4\pi J_\lambda$ obtained from the ISRF, embedded stars, and cloud's radiation; (e) repeat steps (b) through (d). We used three iterations, although the field did not change appreciably after the first.

4.2. *Optical properties of grains in the diffuse* ISM *and in* GMC's

Both the characteristics of the dust grains and the variation of dust opacity with galactocentric distance D_G are discussed in Appendix C. In this subsection we summarize the dust characteristics used in our model computations of GMC's.

In the diffuse ISM the MRN model appears to describe most observed dust characteristics to a good approximation. It is, however, to be expected that inside GMC's, at large values of A_V, the silicate and graphite grains of the diffuse ISM will be coated with ice mantles and the grain size distribution will be different from that in the diffuse ISM. The reasons why we nevertheless use the MRN dust model throughout a GMC are discussed in Appendix C. In summary, most of the stellar radiation shortward of 3 μm is absorbed in the outer sheath of a cloud (i.e. within a layer with an extinction A_V, measured from the surface of the cloud, <3 mag), where dust should still be similar to that in the diffuse ISM. In the center of the cloud, where grains may be coated and where the sizes may be larger, the stellar radiation field is so low that the visual grain properties have little influence on the grain heating. The effect of ice mantles on the FIR absorption could be substantial and the derived dust temperatures for $A_V \gtrsim 25$ mag must be considered quite provisional. But the fact that the MRN dust model approximates the FIR/submm absorption cross sections derived from observations of GMC's reasonably well (Paper I) indicates that changes introduced by ice mantles are not order of magnitude effects.

As in Paper I we make the assumption that the dust-to-gas mass ratio increases proportionally to the heavy element abundance, i.e. $m_d/m_g \propto Z(D_G)/Z_\odot$, and that this increase results in an increase in the number of dust grains rather than in an increase of the size of the dust grains.

4.3. *The radiation field within a* GMC

The mean radiation intensity in a GMC, $4\pi J_\lambda(D_G, A_V)\lambda$, as a function of the visual extinction A_V measured from the surface of a very opaque cloud ($A_{V_0}=200$) is shown in Fig. 4 for $D_G=5$ kpc. Corresponding spectra for $D_G=10$ kpc are very similar in shape. Our treatment of the radiation transfer problem and especially the adopted dust model is not very accurate for $A_V>20$ mag. Therefore, the radiation intensity in Fig. 4 for $A_V=50$ mag should be considered as a qualitative rather than quantitative representation of the spectral change of the radiation field inside GMC's. If the opacity to the center of the cloud, A_{V_0}, is decreased, $4\pi J_\lambda(A_V)\lambda$ for $\lambda \lesssim 100$ μm increases slightly relative to the curves shown in Fig. 4, since at longer wavelengths the cloud becomes more and more transparent. For a similar reason (i.e. since less stellar radiation is converted into FIR/submm radiation) $4\pi J_\lambda(A_V)\lambda$ for $\lambda \gtrsim 100$ μm decreases relative to the curves shown in Fig. 4.

The most obvious feature of the radiation field inside the cloud, shown in Fig. 4, is the very large FIR radiation field, peaking at ~ 200 μm, which is found throughout the cloud. This

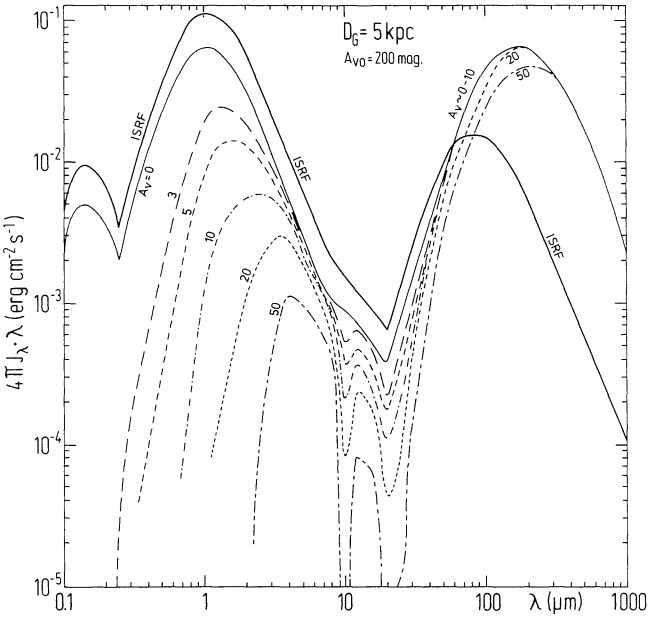

Fig. 4. The radiation field inside a giant molecular cloud, located at $D_G=5$ kpc and with a visual extinction to its center of $A_{V_0}=200$ mag. ISRF refers to the radiation field at far distances from the cloud, $A_V=0$ is the radiation field at the surface of the cloud, $A_V=3$, 5, 10 etc. is the radiation field inside the cloud at distances $A_V=3$, 5, 10 etc. mag from the surface of the cloud

field is much stronger than the Galactic ISRF, which is also shown in Fig. 4, and should be considered in studies of molecular level populations. It also keeps the dust inside the cloud at temperatures well above the 2.9 K background. This rather strong internal radiation field is produced by the conversion in the outer layers of the cloud of all of the incident ISRF to FIR radiation, so its presence is almost independent of our grain model.

Another clear feature shown in Fig. 4 is the rapid drop of $4\pi J_\lambda\lambda$ at ultraviolet wavelengths at different depths in the cloud. At values of $A_V \gg 25$ mag, at which depth the 3.07 μm ice feature is observed, the ultraviolet and visible fields are both very small. Similar absorptions occur at the silicate bands at 10 μm and 20 μm.

Figure 4 also shows the ISRF we calculated at 5 kpc. We see that for $\lambda \lesssim 20$ μm it is about a factor of 2 larger than the radiation field at the surface of the cloud. The reason is that the cloud is opaque to radiation $\lesssim 20$ μm so that the intensity of the ISRF is decreased from $4\pi J_\lambda$ to $2\pi J_\lambda$ and that there is little backward scattering from the cloud at these wavelengths. Even at rather long wavelengths ($\lambda \approx 50$ μm) $4\pi J_\lambda\lambda$ is lower in the cloud than in the ISRF, and only at very FIR wavelengths the cloud emission completely dominates the ISRF.

We note that Fig. 4 displays $4\pi J_\lambda\lambda$, the mean intensity, rather than the flux. Thus, we do not expect any "conservation theorem" to apply, in which a decrease within one spectral region of $4\pi J_\lambda\lambda$ from one point to another in the cloud is necessarily accompanied by an increase to another spectral region; in the classical grey stellar atmosphere, J_λ decreases outwards, although the flux is constant. The fact that all depths in the cloud have the same J_λ for $\lambda > 300$ μm is a related fact; the cloud model is transparent at these wavelengths, so all points can receive radiation radiated

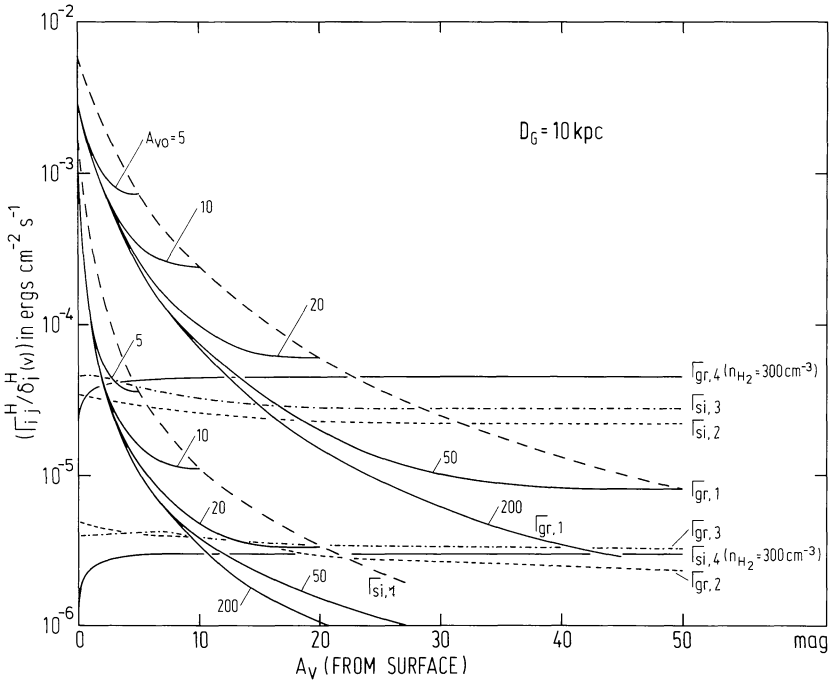

Fig. 5. The heating rate for graphite (gr) and silicate (si) grains as a function of A_V, the extinction in mag measured from the surface of the cloud. Curves labelled $j=1$ give the heating rate due to direct absorption of stellar radiation, $A_{V_0}=5$, 10, 20 etc. refers to clouds with central visual extinctions of A_{V_0} mag. Curves labelled $j=2$ give the heating rate due to absorption of the diffuse galactic FIR radiation, $j=3$ give the heating rate due to absorption of the FIR radiation field of the cloud itself, $j=4$ give the heating rate due to field stars which happen to be embedded in the cloud

from the dust equally well. At deeper depths in the cloud, there is less ultraviolet radiation field, but the reradiated radiation contributes to the J_λ of all of the cloud, but to the flux of only the layers outside the point.

4.4. *Heating rates of dust in* GMC's

In the introduction to this section we listed four radiation fields which are important heating sources for dust grains embedded in GMC's. For the first three, we define for each point inside the cloud characterised by its visual extinction A_V a heating rate per H-atom

$$\Gamma^H_{i,j}(A_V) = \int 4\pi J_{\lambda,j}(A_V, D_G)\sigma^H_{\lambda,i}(D_G)d\lambda \text{ erg s}^{-1}(\text{H-atom})^{-1}. \quad (10)$$

Here i refers to the grain material (graphite or silicates), $j=1, 2, 3$ to the radiation fields which contribute to the heating, dust absorption cross sections are $\sigma^H_{\lambda,i}(D_G)=\sigma^H_{\lambda,i}(\odot)\,Z(D_G)/Z_\odot$ and the radiation field $4\pi J_{\lambda,j}(A_V, D_G)$ is computed analogous to the curves shown in Fig. 4, but separately for the radiation fields $j=1$, 2, and 3. The heating of dust by field stars embedded in a GMC is treated summarily by estimating the emissivity per unit volume of each of the four stellar components ℓ given in Table A1, and solving the equation of radiative transfer as described in Sect. 4.1, to get $I_{\lambda,4}$, the radiation intensity from the embedded stars. Then $4\pi J_{\lambda,4}$ is obtained by integrating over solid angle and, after substitution in Eq. (10), yields $\Gamma^H_{i,4}$.

For the following discussion it is important to see in a straightforward way how $\Gamma^H_{i,4}$ depends on both the stellar emissivity per unit volume and the mean gas density of the cloud in which the stars are embedded. For this purpose we express $\Gamma^H_{i,4}$ in the form

$$\Gamma^H_{i,4} = \sum_\ell \eta_\ell(A_V) n^*_\ell L^*_{\ell,i}/2n_{H_2}, \quad (10b)$$

where i refers to the grain material, $L^*_{\ell,i}$ is that part of the total stellar luminosity L^*_ℓ absorbed by grains of material i, and $\eta_\ell(A_V)\leqq 1$ is the fraction of stellar radiation which is absorbed by dust in the cloud. From this relation it is clear that $\Gamma^H_{i,4}$ decreases with the average gas density of the cloud and increases with the stellar emissivity per unit volume. Considering only MS stars of the disk population we feel that the number density of stars of stellar components $\ell=1$ (OB stars) and $\ell=4$ (red giants, supergiants) is probably so small that chances of their fortuitous association with GMC's are negligible. We therefore consider heating only from stars of components $\ell=2$ and 3, which have the same volume density in GMC's and in the diffuse ISM, respectively. Of course, since most OB stars form in GMC's there is a generic association of these stars with GMC's. But as will be discussed in Sect. 5.2, heating of dust by OB stars can apply only to a small fraction of all GMC's in the Galaxy. The space density of recently formed lower mass stars, which are still on their pre MS contraction, on the other hand, could be quite high in GMC's with high star formation rates. In such clouds embedded stars may become an important heating source for the dust.

As an illustration of the relative importance of the four sources of heating we have plotted in Fig. 5 the dominant heating rates for both graphite and silicate grains as a function of A_V, the extinction measured from the surface of the clouds, considering clouds with different central extinction A_{V_0}. The ISRF is that for the solar vicinity ($D_G=10$ kpc). A similar diagram for $D_G=5$ kpc shows qualitatively the same behavior. Displayed in Fig. 5 are not the heating rates per H-atom, $\Gamma^H_{i,j}$, but rather the quantity $\Gamma^H_{i,j}/\sigma^H_V$, which is the heating per visual optical depth. Multiplied with $d\tau_V=2n_{H_2}\sigma^H_V ds$, this is the heating rate of a volume of 1 cm^2 cross-section and a length ds corresponding to the visual extinction depth $d\tau_V$. The behavior of these curves follows from the wavelength dependence of the absorption cross sections of graphite and silicate grains as shown in Fig. 1 of Paper I and the radiation field inside a GMC as shown in Fig. 4 of this paper. The dashed lines labelled $\Gamma_{i,1}$ show the heating rate at the center of a cloud with A_{V_0} equal to A_V (from surface). The solid lines labelled $\Gamma_{i,1}$ and A_{V_0} show the heating rate as a function of visual extinction A_V for clouds with central opacities $A_{V_0}=5, 10\ldots$mag.

Since graphite grains absorb best at wavelengths $\lesssim 10\,\mu m$, their stellar heating rate $\Gamma_{gr,1}$ is always dominated by radiation from stars of stellar components 2, 3, and 4. Since the mean intensity of the ISRF peaks at $\sim 1\,\mu m$, at which wavelength a standard GMC is already rather transparent $\Gamma_{gr,1}$ is the dominant heating rate for graphite grains at $A_V \lesssim 20$ mag from the surface of the cloud. Deeper inside the cloud the heating of embedded stars of stellar components 2 and 3 becomes more important. Note, however, that according to Eq. (10) the $\Gamma^H_{i,j}$ for $j=1, 2, 3$ stay constant, while $\Gamma^H_{i,4}$ decreases $\propto n_{H_2}^{-1}$. In Fig. 5 Γ^H_{gr}, the heating rates by embedded stars relate to the gas density $n_{H_2} = 300\,cm^{-3}$ of a standard GMC. Since large values of the central cloud extinction A_{V_0} usually go with high gas densities n_{H_2}, the heating of graphite grains by the ISRF may even dominate for clouds with $A_{V_0} = 50$ mag. FIR heating becomes important only for very opaque clouds ($A_{V_0} > 50$ mag) and at distances below the cloud surfaces corresponding to $A_V \gtrsim 40$ mag. On the other hand, if many low-mass stars form in quiescent GMC's of moderate density (as may be the case for dust clouds associated with T Tauri star associations), their radiation could be important contributors to the heating of graphite grains.

Silicate grains absorb better than graphite in the far UV and in the far IR. In the outer sheath of the cloud ($A_V \lesssim 2$ mag) the heating rate is dominated by OB stars (stellar component 1). Farther inside the cloud, heating by FIR radiation takes over. The heating rate $\Gamma_{si,2}$ for the FIR radiation field of the cloud itself is slightly higher than the heating rate $\Gamma_{si,3}$ for the diffuse galactic FIR radiation.

4.5. Dust temperatures

With the notation of heating and cooling rates used in this paper Eqs. (6) through (9) of Paper I can be rewritten in the form

$$\sum_{j=1}^{4} \Gamma^H_{i,j} = \Lambda^H_i(T_i) \tag{11}$$

with the cooling rate

$$\left[\frac{\Lambda^H_i(T_i)}{\text{erg s}^{-1}\text{(H-atom)}^{-1}}\right] = 3.49\,10^{-5}\left[\frac{\sigma^H_{\lambda_1}(i)}{\text{cm}^2\text{(H-atom)}^{-1}}\right] \cdot \left[6.95\,10^{-5}\frac{\lambda_1(i)}{\mu m}\right]^m \left[\frac{T_i}{K}\right]^{4+m} \phi(m). \tag{12}$$

Here m, $\phi(m)$, $\lambda(i)$, and $\sigma^H_{\lambda_1}(i)$ are related to the FIR emission properties of the grain species i and are taken from Table 3, Paper I. In the diffuse ISM only the direct heating by starlight, i.e. $\Gamma_{i,1}$ in Eq. (11), has to be considered. The corresponding grain temperatures T_i(H I) are shown as a function of D_G in Fig. 3.

In Fig. 6a and b are plotted grain temperatures as a function of A_V, measured from the surface of the cloud, for clouds of different central visual extinction A_{V_0} and for the galactocentric distances $D_G \doteq 10$ and 5 kpc. Dashed lines refer to the center of clouds with $A_{V_0} = A_V$, while solid lines refer to the dust temperature of clouds with a central visual extinction as labelled. The different temperatures of graphite and silicate grains and their different variation inside a GMC are readily explained by the heating rates (Fig. 5) and the fact that the FIR absorption cross-sections of graphite are about one order of magnitude lower than those of silicates. Since silicate grains absorb less stellar radiation and emit more FIR radiation, their temperature in the diffuse ISM and in the outer sheath of GMC's are about a factor of two lower than those of graphite grains. The dominant heating source of graphite grains is

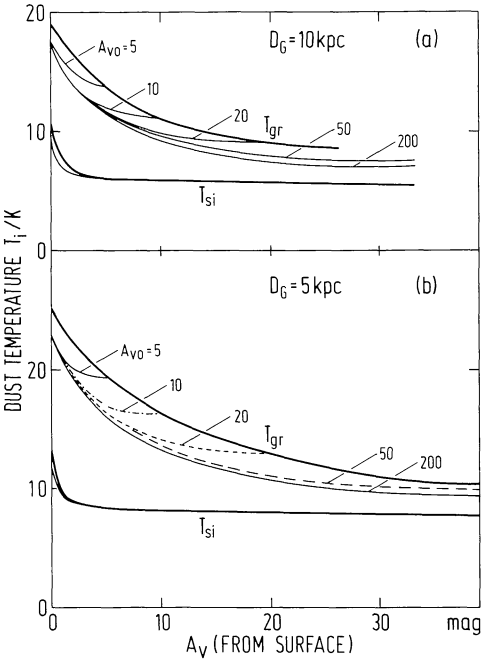

Fig. 6a and b. Temperatures of graphite (gr) and silicate (si) grains in giant molecular clouds given as a function of A_V, the visual extinction measured from the surface of the cloud. Diagram **a** holds for the galactocentric distance $D_G = 10$ kpc and diagram **b** for $D_G = 5$ kpc. Dashed lines refer to the center of clouds with $A_{V_0} = A_V$, solid lines refer to the center of clouds with central opacity as labelled

direct stellar radiation and T_{gr} therefore decreases approximately with the 1/6 power of the integrated stellar radiation intensity (Fig. 4). The temperature of silicate grains is determined by direct stellar radiation only in the very outer layers of a GMC. At $A_v \gtrsim 2$ mag heating by FIR radiation dominates. Since the intensity of the FIR fields stays nearly constant inside a GMC (see Fig. 4), the temperature of silicate grains is practically constant, too, and is about 6 K at $D_G = 10$ kpc and 8 K at $D_G = 5$ kpc. If gas were thermally coupled to the dust it would assume a temperature T_K somewhere between that of graphite and silicate grains. It is of interest to note that for the interior of a standard GMC located at $D_G \sim 5$ kpc this would mean $13\,K > T_K > 8\,K$, which agrees well with temperature estimates from CO line observations, $\langle T_K(\text{GMC})\rangle \sim 10$ K.

In Fig. 6 we did not consider heating by stars embedded in the GMC. It will always be unimportant for silicate grains because they do not readily absorb visual radiation. It will stabilize the temperature of graphite grains at about the value where $\Gamma_{gr,1} \sim \Gamma_{gr,4}\,(300/n_{H_2})$ if we take the numerical value of $\Gamma_{gr,4}$ from Fig. 5. Without heating by embedded stars and for very opaque clouds the temperature of graphite grains gradually approaches that of silicate grains. At the center of a cloud with $A_{V_0} = 200$ mag we have $T_{gr} = 5.5$ K, $T_{si} = 5.1$ K for $D_G = 10$ kpc and 7.8 and 7.1 K at 5 kpc, respectively. The reason is that in the FIR, where now the grains both absorb and emit, the absorption cross sections of graphite and silicate run nearly parallel (see Fig. 1 of Paper I) and that $T_i \propto (\sigma^i_{abs}/\sigma^i_{em})^{1/6}$.

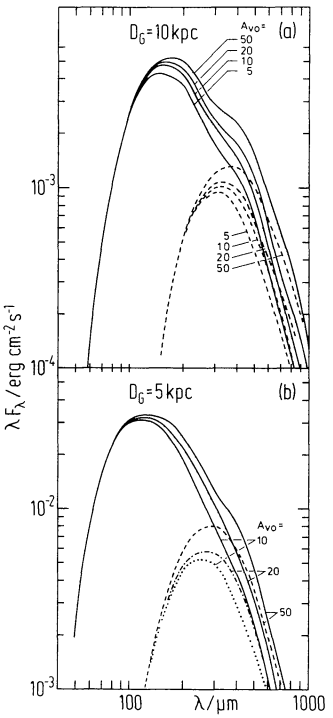

Fig. 7a and b. The flux density of giant molecular clouds located at galactocentric distances $D_G = 10$ kpc **a** and 5 kpc **b**, respectively, given as function of their central opacity A_{V_0}. Solid lines relate to the emission of both graphite and silicate grains, dashed curves relate to the emission of silicate grains only

In Fig. 7a and b is plotted the flux F_λ in erg s^{-1} μm^{-1} cm^{-2} which is emitted from the cloud, multiplied by the wavelength λ. Solid curves relate to the emission of both graphite and silicate grains, dashed curves relate to the emission from silicate grains only. The emission from graphite grains contains about five times the energy emitted by silicate grains. The similarity of the emission spectra of clouds with, say, $A_{V_0} = 5$ and 50 mag shows that attempts to estimate dust masses by fitting model spectra to observations will be futile. Since only a thin outer sheath of the molecular cloud absorbes and reradiates practically all of the ISRF, the total flux emitted by a cloud is proportional to its surface, i.e. in the case of a spherical cloud $S_\nu \propto R^2$, with R the clouds radius. Only at wavelengths $\gtrsim 200$ μm does the cool dust inside the cloud start to contribute to the emission spectra and the surface brightness begins to depend on the total column density of dust.

In Fig. 3 are plotted, as a function of D_G, characteristic dust temperatures of graphite and silicate grains in standard GMC's of $A_{V_0} = 20$ mag, which are obtained by fitting modified Planck functions $B_\lambda(T_i)\lambda^{-2}$ to the computed cloud spectra (open circles). They are compared to the simple approximation $T_i(\text{cloud}) \sim (0.5\, e^{-1})^{1/6} T_i(\text{H I})$ (dashed curves), which assumes that the emission spectrum of a cloud is determined by dust at a depth $\tau_\lambda \sim 1$ below the surface, with λ the wavelength of the absorbed radiation (Bollea and Cavaliere, 1976). While this is a good approximation for the emission spectrum of silicate grains it yields too low values for graphite grains, probably since a cloud with $A_{V_0} = 20$ mag is still transparent to the NIR part of the ISRF, which contributes strongly to the heating of graphite grains.

5. Discussion and conclusions

On the basis of the results obtained in the previous sections we address here some problems related to the nature of the four stellar components, the origin of the diffuse galactic FIR/submm emission and the intensity of the FIR field inside and near GMC's and its representation by diluted Planck curves. In the last subsection we discuss qualitatively the luminosity and spectrum of the dust emission from protostars embedded in GMC's.

5.1. *The nature of the stellar components*

In Sect. 1 and Appendix A we considered four stellar components, whose characteristics are summarized in Tables A1 and A2. Remember that components $\ell = 1$, 2, and 3 have been introduced to explain the intensity of the ISRF as observed for $\lambda < 1$ μm in the solar vicinity. The variation of the stellar emissivities with galactocentric distance have been inferred from radio observations of the free-free emission (component 1) and from optical observations of the variation of the surface brightness of external galaxies (components 2 and 3). For component 4 both $j_4^\odot$ and α_4 were obtained from a model fit to the mean radiation intensity $4\pi J^\odot_{2.4\,\mu m}$ and the ridge line intensity $I^\odot_{2.4\,\mu m}(l, b = 0°)$ observed for the solar vicinity.

Galactic luminosities given in Table 1 are obtained by integration of the volume emissivities

$$L_\ell = 4\pi \int_{D_{\min}}^{D_G = 13\,\text{kpc}} 4\pi j_\ell(0) e^{-\alpha_\ell r} H_\ell r dr \,. \tag{13}$$

The total luminosity produced by stars of the galactic disk for $D_G \lesssim 13$ kpc and $\lambda \gtrsim 0.09$ μm is then $L_{\text{tot}} = \sum_{\ell=1}^{4} L_\ell \sim 5\,10^{10} L_\odot$. To obtain the optical luminosity of the galactic disk we have to subtract $1\text{E}10\, L_\odot$ of star light which is absorbed by dust and reradiated in the FIR. This luminosity compares well with the estimate given in Paper I, $L_{\text{tot}} = 4\,10^{10} L_\odot$ (Tamman, priv. comm.). Further, we have estimated $L_{1,\lambda>0.09} = 3.6\,10^9 L_\odot$ in Paper I. The lower luminosity of component 1 (OB stars) given in Table 1 is due to the fact that the UV part of the ISRF has been adjusted to observations in the solar vicinity where the OB star density is certainly lower than average, since most of the massive stars form in the main spiral arms.

A riddle is the existence of component 4, which apparently consists of M-type giants and supergiants with surface temperatures of ~3000 K. Since $L_4 \sim 5 L_1$ (Table 1), only a minor fraction of these stars can be M supergiants which originate from evolved, massive OB stars. The larger Z abundance at $D_G \approx 5$ kpc can increase the relative lifetime of a star in the red supergiant phase (Guiderdoni and Rocca-Volmerange, 1982), but this effect is not enough. Serra et al. (1980) suggest that component 4 consists

Table 1. Luminosities of stellar components $l = 1 \ldots 4$

ℓ	H_ℓ/pc	$j_{o\ell}$/erg cm^{-3} s^{-1}	$L_\ell(D_G = 0\text{-}13\ \text{kpc})/L_\odot$
1	60	1.0(-23)	2.3(9)
2	190	5.9(-24)	1.8(10)
3	270	4.3(-24)	1.9(10)
4	50	4.8(-22)	1.1(10)

primarily of M giants with MS lifetimes of $3\,10^8$–$3\,10^9$ yr, which have masses in the range 1.5–3 $M_\odot$. However, the extremely high volume emissivities of these stars can only be explained if the star formation rate some 10^9 yr ago was considerably higher than today (at least 30 times that in the solar vicinity or 5 times that observed today for $D_G = 5$ kpc).

5.2. *The origin of the diffuse galactic* FIR/submm *emission*

The total luminosity of the diffuse galactic FIR/submm for $\gtrsim 50$ μm is $\sim 6\,10^9\,L_\odot$. The origin of this diffuse emission was the main topic of Paper I. There we concluded that the temperature of dust associated with atomic hydrogen was nearly independent of galactocentric distance. The corresponding temperature values are indicated in Fig. 3 by $T_i^{\rm I}$(H I). With these dust temperatures we found that dust associated with atomic hydrogen could only account for ~20% of the total FIR luminosity, while dust associated with molecular hydrogen could account for less than 7%. I.e. dust associated with neutral hydrogen and heated by the general ISRF did neither provide enough luminosity nor did it yield the right spectral distribution to explain the observed diffuse galactic FIR/submm emission. That is why we had to postulate that most of the diffuse galactic FIR emission, whose intensity $I_\lambda\lambda$ peaks at $\lambda \sim 80$ μm, originates from dust located in extended low-density (ELD) H II regions and heated by O stars. In this paper we derive an ISRF whose intensity in the solar vicinity is ~30% higher than that used in Paper I, which in addition increases by about a factor of seven from $D_G = 10$ kpc to $D_G = 5$ kpc. As shown in Fig. 3, this results in considerably higher temperatures of dust associated with neutral hydrogen and, of course, must increase the contribution of this dust component to the observed diffuse FIR/submm emission.

Recently, Smith (1982) has mapped the FIR emission of M 51. He finds a total luminosity of $2\,10^{10}\,L_\odot$ of which about one third is emitted from the central part of the galaxy. Thus the conditions appear to be rather similar to our Galaxy (Mezger, 1983). The low dust temperature derived for the central part of M 51, ~20 K, indicates that most of the dust is heated by the ISRF.

The heavy curve in Fig. 8, labelled (PS), is the spectrum of the diffuse galactic emission observed in the direction $l \sim 30°$, $b \sim 0°$, the dashed curves labelled (1) and (2) refer to the emission spectra of dust associated with atomic hydrogen and ionized hydrogen in ELD H II regions, as estimated (and displayed in Fig. 3) of Paper I.

We have recomputed the emission spectrum of dust associated with atomic hydrogen in the direction $l \sim 30°$, $b \sim 0°$ using the ISRF derived in this paper. The result is shown as solid curve (1) in Fig. 8. As to be expected, the spectrum is (compared to the corresponding dashed curve) shifted towards shorter wavelengths and its peak intensity is increased by about a factor of two. Emission from this dust component now accounts for ~40% of the total diffuse FIR/submm emission. The contribution from dust heated by OB stars [solid curve (2)] is decreased accordingly, this dust component accounting now for 60% of the total diffuse emission (as compared to 80% in Paper I). It is generally accepted that only O stars can heat dust grains to the temperatures required to fit the observed peak emission shortward of 100 μm. However, it is not yet fully recognized that this cannot be done by O stars in their earliest cocoon stages, where they are still fully embedded in GMC's and have not yet created an H II region [a case, which has been numerically investigated by Natta et al. (1981)]. The reason is that the lifetime of these cocoon stars can only be a minor fraction of the MS lifetime of O stars. The fraction

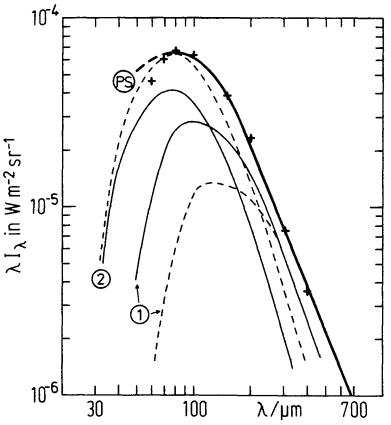

Fig. 8. The emission spectrum of our Galaxy observed in the direction $l \sim 30°$, $b = 0°$ (Paper I). Curve (1) relates to the contribution from dust associated with the diffuse ISM (atomic hydrogen), Curve (2) relates to the contribution from dust associated with ionized gas in ELD H II regions. Dashed curves are from Paper I, solid curves relate to model computations from this paper

of the total luminosity $L_{\rm IR}$ of the diffuse galactic emission, $\sim 0.6\,L_{\rm IR} = 3.6\,10^9\,L_\odot$, has to be compared with the total luminosity of all O stars in the Galaxy, $\sim 7\,10^9\,L_\odot$ (Paper I). Obviously one needs at least one half of all galaetic O stars to account for this luminosity. Since O stars spend most of their lifetime ionizing evolved ELD H II regions, dust associated with these regions is the most likely source for the diffuse emission shortward of 100 μm. This implication is not at all in contradiction with the observed good correlation in galactic longitude between FIR emission and the emission of the rotational lines of the CO molecule (which is usually used to derive H_2 column densities). After all, these quantities also correlate well with the longitudinal distribution of the diffuse radio free-free emission (Mezger, 1978). It just shows that O stars form predominantly in GMC's and spend a good fraction of their lifetime trying to rid themselves of their parental molecular clouds.

What fraction of GMC's are quiescent, i.e. are not heated by O stars? In Paper I we have estimated the total mass of (as we feel predominantly ionized) gas associated with warm dust (i.e. $T_{\rm gr} \sim 40$ K, $T_{\rm si} \sim 29$ K), which is responsible for most of the galactic FIR emission, to be $2.9\,10^7\,M_\odot$. This mass should now be reduced by a factor 0.6. Compared with Güsten's estimate of the total mass of molecular hydrogen, $\sim 6\,10^8\,M_\odot$, this warm dust accounts for less than 3% of the total mass of dust associated with GMC's. This means that even if all O stars were embedded in GMC's, their radiation could only heat a minor fraction of the total dust mass contained in GMC's. Conditions envisaged here for "quiescent GMC's", therefore probably apply to more than 90% of the total gas contained in the galactic disk in the form of molecular hydrogen.

5.3. *The* FIR *field inside or near* GMC's

The mean radiation intensity at the surface and at various depths inside a very opaque GMC at $D_G = 5$ kpc is shown in Fig. 4. Qualitatively, the radiation field in less opaque clouds and in clouds at different galactocentric distances looks similar, as

Table 2. Representation of the FIR field in GMC's at $D_G = 5$ kpc by diluted blackbody radiation

i	T	W	Scaling factor for W
5	40	$2.5\ 10^{-5}$	$R_{Dust}(D_G)/R_{Dust}(5\ kpc)$
6	24	$1.0\ 10^{-3}$	$R_{st}(D_G)/R_{st}(5\ kpc)$
7	10	$6.0\ 10^{-3}$	

discussed in Sect. 4.3. A salient feature is that for $\lambda \gtrsim 40\ \mu m$ the intensity of the radiation field at the surface and inside a GMC is nearly constant and, to a good approximation, can be described by the superposition of the ISRF and two times the computed flux density of a cloud as shown, for example, in Fig. 7. The reason is that most of the ISRF for wavelengths $\lesssim 30\ \mu m$ gets absorbed by dust in the outer sheaths of a GMC, from which it is reemitted as FIR/submm radiation, for which even a very opaque cloud is quite transparent. Thus at any point inside a GMC one sees a warm but optically thin wall whose emission is given by diluted Planck function temperatures T_{gr}(GMC) and T_{si}(GMC), as shown as a function of D_G in Fig. 3.

Such a strong FIR field may affect the population of energy levels in a molecule and induce non-LTE effects in their radio line emission. For numerical computations of such effects it is convenient to approximate the FIR part of the radiation by three diluted Planck functions, $I_{\lambda>20\,\mu m} = \sum_{i=5}^{7} W_i B_\lambda(T_i)$. Temperatures and dilution factors for $D_G = 5$ kpc are given in Table 2. The diluted 40 K blackbody radiation field represents the diffuse galactic FIR emission and its dilution factor therefore scales with $R_{Dust}(D_G)$ as given by Eq. (6) and Fig. 2b. The diluted 24 and 10 K blackbody radiation fields represent the ISRF which is converted into FIR/submm radiation in the outer layers of the cloud. Their dilution factors scale with $R_{st}(D_G)$ as given by Eq. (3b) and Fig. 2a.

5.4. *The emission spectra of dense condensations inside* GMC's

The earliest evolutionary phases of star formation consist of isothermal contraction and fragmentation. They are associated with gas densities $n_H \sim 10^6$–$10^9\ cm^{-3}$. Thermal radiation from dust grains offers a possibility to observe these evolutionary stages. Our previous results allow a guess of the spectrum and flux density emitted by such a condensation. Let us consider a protostar of mass $M_{pr} = X^{-1} M_H$, with M_H its hydrogen mass, n_H the hydrogen density and $X (\sim 0.70$ in the solar vicinity) the mass fraction of H. Numerical estimates relate to the solar vicinity (i.e. $D_G = 10$ kpc). The radius of the protostar is

$$R = 6.57\ 10^{18} (M_H/n_H)^{1/3}\ cm$$
$$= 2.13 (M_H/n_H)^{1/3}\ pc \qquad (14)$$

with M_H in solar masses and n_H in cm^{-3}. The visual extinction to the center of the protostar is

$$A_{V,pr} = 1.086\, R n_H \sigma^H_{V,ext} = 3.81\ 10^{-3} (M_H n_H^2)^{1/3}\ mag \qquad (15)$$

if its extinction per H atom is the same as in the diffuse ISM. Its angular diameter, seen from a distance D (in kpc), is

$$\left[\frac{\theta_s}{arc\ s}\right] = \frac{2R}{D} = 8.79\ 10^2\, D^{-1} (M_H/n_H)^{1/3}. \qquad (16)$$

If, like a globule, it is directly exposed to the ISRF its luminosity would be

$$\left[\frac{L_{pr}}{L_\odot}\right] = \pi R^2 \int_0^\infty 4\pi J_\lambda d\lambda = 7.68\ 10^2 (M_H/n_H)^{2/3} \qquad (17)$$

i.e. it would decrease $\propto R^2 \propto (M_H/n_H)^{2/3}$, since most of the ISRF is absorbed in the outer layers of the protostar. Hence, the FIR/submm emission scales with the surface of the cloud. The spectrum would be given by Fig. 7a. As an example, we consider a protostar with $M_{pr} = X^{-1} M_H = 1\, M_\odot$ and $A_{V,pr} = 30$ mag. Its density is $n_H \simeq 10^6\ cm^{-3}$, its angular diameter is $\theta_s \simeq 8\, D^{-1}$ arc s and its luminosity is $L_{pr} \simeq 6.1\ 10^{-2}\, L_\odot$, if the protostar is located in the open interstellar space. However, it is probable that the protostar is located inside a molecular cloud. We consider therefore the same protostar located in a cloud of $A_{V_0} = 20$ mag at a depth $A_V = 10$ mag from the surface of the cloud. From Fig. 4 we see that the ISRF at $A_V \sim 10$ mag attains its maximum at $\lambda \sim 2.4\ \mu m$, where the optical absorption depth of the protostar is ~ 2. While the temperature of graphite grains (which are heated by the direct stellar radiation) decreases from ~ 10 K at $A_V = 10$ to ~ 8.5 K at $A_V + A_{V_0} = 30$ mag (see Fig. 6a), the temperature of silicate grains (which are heated by FIR radiation emitted by dust grains in the outer layers of the cloud) is rather constant and ~ 6 K.

Since there is no strong variation of the grain temperature all grains contribute about equally to the emission from the protostar whose luminosity therefore is proportional to $\mathfrak{N}_H = M_H/m_H = 1.19\ 10^{57}\, M_H$, the total number of H-atoms contained in the protostar:

$$\left[\frac{L_{pr}}{L_\odot}\right] = \mathfrak{N}_H \sum_{i=1}^{2} \Lambda_i^H(T_i)$$
$$= 3.11\ 10^{23}\, M_H [1.89\ 10^{-32}\, T_{gr}^{6.2} + 4.78\ 10^{-31}\, T_{si}^{6.3}]$$

with $\Lambda_i^H(T_i)$ from Eq. (12), M_H in $M_\odot$, T_i in K. Adopting for $T_{gr} = 9$ K, $T_{si} = 6$ K we obtain $L_{pr} \sim 1.7\ 10^{-2}\, L_\odot$, which is about a factor of ~ 4 less than the luminosity of the same protostar exposed to the unattenuated ISRF. However, while in the latter case graphite grains contribute $\sim 5/6$ and silicate $\sim 1/6$ to the protostars luminosity our estimate for the same protostar located at $A_V \sim 10$ mag inside an extended molecular suggests that now graphite grains contribute $\sim 1/3$ and silicate grains $\sim 2/3$ to the luminosity. Therefore, the emission spectrum should be dominated by silicate grains and the protostar should emit its maximum flux density between ~ 200 and $\sim 800\ \mu m$, a wavelength range which for $\lambda \gtrsim 350\ \mu m$ is accessible to earthbound observations. With the next generation of mm/submm radiotelescopes, such as the MPIfR/IRAM 30-m MRT or the MPIfR/Univ. of Arizona 10-m SMT, which both have an angular resolution of $\theta_A \sim 10''$ at their minimum wavelengths of 1000 μm and 350 μm, respectively, it should in fact be possible to detect protostars embedded in giant molecular clouds.

For continuum observations one operates the telescope in the beam switching mode, where the telescope beam successively points at the protostar and at the surface of the cloud beside the protostar. With I_{pr} the surface brightness seen in the direction of the protostar embedded in the cloud and I_{cl} the surface brightness of the cloud the telescope measures the flux density

$$\Delta S = \frac{I_{pr} - I_{cl}}{I_{cl}} I_{cl} \Omega_s. \qquad (18)$$

As before we consider the case of a protostar of $M_{pr} = 1\, M_\odot$ with central visual extinction $A_{V,pr} = 30$ mag embedded in a molecular

Table 3. Surface brightness and flux density of a protostar of $M_{pr}=1\,M_\odot$ and $A_{V,pr}=30$ mag embedded in a molecular cloud of $A_{V_0}=20$ mag at a depth $A_V=10$ mag below the surface

Wavelength and frequency		$(I_{pr}-I_{cl})/I_{cl}$		I_{cl} (10^{-5} erg cm^{-2} s^{-1} sr^{-1} μm^{-1})		(ΔS/Jy) (D/kpc)^2	
λ/μm	ν/10^{12} Hz	D_G=10 kpc	5 kpc	10 kpc	5 kpc	10 kpc	5 kpc
80	3.75	−0.15	−0.16	0.188	4.15	−0.001	−0.017
90	3.3	−0.12	−0.14	0.294	4.89	−0.001	−0.022
100	3.0	−0.08	−0.11	0.408	5.35	−0.001	−0.024
150	2.0	0.14	0.04	0.713	4.56	+0.009	+0.016
200	1.5	0.35	0.24	0.593	2.80	+0.033	+0.107
300	1.0	0.67	0.65	0.244	1.00	+0.058	+0.234
400	0.75	0.87	0.85	0.156	0.51	+0.087	+0.277
600	0.50	1.10	1.07	0.039	0.10	+0.062	+0.154
800	0.38	1.18	1.15	0.012	0.026	+0.036	+0.077
1000	0.30	1.24	1.20	0.004	0.008	+0.020	+0.036

cloud of $A_{V_0}=20$ mag at $A_V=10$ mag below the surface of the cloud. It follows from Eqs. (14) through (16) $n_H\sim10^6$ cm^{-3}, $R\sim2\,10^{-2}$ pc, $\theta_s\sim8''\,D^{-1}$ and $\Omega_s\sim\pi(\theta_s/2)^2=1.2\,10^{-9}$ $(D/\mathrm{kpc})^{-2}$ sr. However, now we use the results of the rigorous radiative transfer computations outlined in Sect. 4.1. The quantities which enter into Eq. (18) have been computed for a protostar with the characteristics given above and are given in Table 3. Note that $(I_{pr}-I_{cl})/I_{cl}$ becomes negative at $\lambda<150$ μm since the protostar becomes opaque and thus blocks more radiation from the rear side of the cloud than it emits.

The luminosity of the protostar,

$$\left[\frac{L_{pr}}{L_\odot}\right]=\frac{4\pi D^2}{L_\odot}\int S_\nu d\nu=2.42\,10^{-2} \tag{19}$$

is about 40% higher than the approximate estimate, Eq. (17), where we used single temperatures to characterize the emission of graphite and silicate grains, respectively. This is because the rigorous calculations, allowing for temperature gradients, lead to a spectrum which for each dust component is somewhat broader than a modified Planck function.

In summary, a protostar of $1\,M_\odot$, embedded deeply inside a giant molecular cloud and at a distance of ∼1 kpc from the sun, will have an apparent diameter of ∼10″, a total luminosity of $\sim0.02\,L_\odot$ and a flux density of ∼80 and ∼20 mJy at 350 μm and 1000 μm, respectively. While it would be difficult to detect such an object with the submm telescopes used at present (i.e. mostly optical telescopes with diameters $\lesssim5$ m) its detection with the 30-m MRT or with the 10-m SMT appears to be feasible. With a ^{3}He cooled Ge bolometer in a 1.5-m telescope, placed on Mt. Lemmon we can detect at λ1 mm with an integration time of ∼30 min point sources with flux densities of ∼5 Jy against the general galactic background emission. Using the same bolometer in a 30-m telescope will increase the sensitivity to point sources by a factor ∼400 and the angular resolution of the telescope will just be adequate to include the protostar in the main beam, so that full use of beam-switching technique can be made. Based on this estimate we conclude that it should become possible to detect protostars in their free-fall contraction stage by observing their thermal dust emission in the submm range.

Acknowledgements. J.S.M. appreciates the support of the Alexander-von-Humboldt Foundation of the Federal Republic of Germany by a U.S. Senior Scientist Award, and the U.S. National Science Foundation under grant AST-8117972. The first draft of this paper was completed while P.G.M. was a guest scientist at the Steward Observatory of the U. of Arizona. We have benefitted from discussions with R. Chini, R. Güsten, E. Krügel, and C. Walmsley. We appreciate W.G. Roberge's kindly providing details of the numerical solution of the radiation field inside a uniform dust cloud.

Appendix A: the ISRF from λ0.09 μm to λ8 μm

The ISRF in the solar vicinity was reevaluated in Appendix C (see Table C1) of Paper I. Longward of 0.25 μm the ISRF was approximated by diluted blackbody emissions corresponding to temperatures of 7500 K and 4000 K, respectively, following the procedure of Werner and Salpeter (1969) but slightly altering the dilution coefficients.

Jura (1979) pointed out that the Werner-Salpeter ISRF considerably underestimates the ISRF longward of ∼1 μm, if the NIR emission from the galactic plane as observed by different Japanese groups (see, for example, the review by Okuda, 1980) is properly taken into account. To do this we evaluate the integral

$$4\pi J^\odot_{2.4}=\int_0^{2\pi}dl\,2\int_0^{\pi/2}I_{2.4}(l,b)\cos b\,db \tag{A1}$$

with l, b galactic coordinates. As in Paper I, Eq. (C1), we describe the latitude distribution in terms of an infinite plane parallel slab model which gives $I(b)\propto1-\exp\{-\tau/\sin b\}$. For the absorption optical depth perpendicular to the galactic plane at λ2.4 μm we substitute for the solar vicinity the value $\tau^\odot_{2.4}=0.0127$ which follows from the dust opacity estimated in Appendix C of this paper and adopting a scale height of the dust of 130 pc. Evaluation of the integral yields $2\int_0^1(1-\exp\{-\tau/\mu\}\,d\mu=0.111$ rad.

The ridge line intensity $I(l,b=0°)$ is taken from observations as summarized by Hayakawa et al. (1978) assuming that it is symmetric with respect to $l=0°$. To account for the finite angular resolution (i.e. of a square beam of width 2°) we increase the observed ridge line intensity by a factor a. with

$$a^{-1}(x)=\int_0^{\sin1°}(1-e^{-\tau/\mu})d\mu\Big/\int_0^{\sin1°}d\mu$$
$$=[1-e^{-x}+xE_1(x)] \tag{A2}$$

and

$$x=\tau/\sin1°=57.3\tau$$

For $\tau^\odot_{2.4}=0.0127$ [Eq. (A2)] takes the value $a=1.29$. Integration of the ridge line intensity yields

$$2\int_0^\pi I_{2.4}(l,b=0°)dl=1.2\,10^{-2}\ \mathrm{erg\,cm^{-2}\,s^{-1}\,\mu m^{-1}\,rad^{-1}}.$$

Substituting these values in Eq. (A1) we obtain for the mean radiation intensity at λ2.4 μm

$$4\pi J^\odot_{2.4}=1.89\,10^{-3}\ \mathrm{erg\,cm^{-2}\,s^{-1}\,\mu m^{-1}} \tag{A3}$$

a value which is a factor 1.9 higher than the value derived in Paper I (Appendix C). Note that values $4\pi J^\odot_\lambda$ given in Paper I for $\lambda\gtrsim1$ μm were not based on observations but represent an extrapolation of the ISRF as observed for $\lambda\lesssim1$ μm. The same difference holds for the mean radiation intensity at λ3.4 μm, if the observations by Hayakawa et al. (1980) are used. Most of the

ISRF at 2.4 and 3.4 μm, respectively, is attributed to a new population of red giants (e.g. Hayakawa et al., 1977). To explain the observed ridge line intensity, this red giant population (in the following referred to as stellar component 4) must in essence be concentrated between galactocentric distances $D_G = 4$–8 kpc. Therefore, to account for their emission in the solar neighbourhood, we add to the three components already given in Paper I a fourth component, described by a black body of $T_4 = 3000$ K (as suggested by Price (1981)) and a dilution factor $W_4 = 4.0\,10^{-13}$. Moreover, in order to satisfy the ISRF observed for $\lambda < 1$ μm, we must decrease the contribution of the third stellar component, which in Paper I was described by a black body of $T_3 = 4000$ K and a dilution factor of $W_3 = 1.65\,10^{-13}$. (Note that components 2 and 3 of this paper were labelled components 1 and 2 in Paper I.) The required decrease is achieved by a dilution factor $W_3 = 1.00\,10^{-13}$.

In summary, the stellar contribution to the ISRF consists of four components, in the following labelled by the subscript ℓ:

1. UV emission from early type stars, which dominates the ISRF between 0.09 and 0.25 μm. Its spectrum is that given in Table C1 of Paper I after subtraction of the diluted blackbody emission from components 2, 3, and 4.

2. and 3. Emission due to disk stars, described by diluted blackbody radiation with $T_2 = 7500$ K, $W_2 = 1.00\,10^{-14}$ and $T_3 = 4000$ K, $W_3 = 1.00\,10^{-13}$, respectively.

4. Emission due to Red Giants (or supergiants?), described by blackbody radiation with $T_4 = 3000$ K and $W_4 = 4.0\,10^{-13}$.

The ISRF produced by these four stellar components in the solar neighbourhood, $4\pi J_\lambda^\odot$, is listed in Table A3 for $D_G = 10$ kpc. The individual contributions of the four components as well as the resulting total intensity are shown in Fig. 1. The integrated mean radiation intensity is

$$\int_{0.09}^{8\,\mu m} 4\pi J_\lambda^\odot d\lambda = 2.17\,10^{-2}\ \mathrm{erg\,cm^{-2}\,s^{-1}} \qquad \text{(A4)}$$

which is 28% higher than the value of $1.69\,10^{-1}$ erg cm^{-2} s^{-1} derived in Paper I.

Next we consider the dependence of this stellar ISRF on the galactocentric distance D_G. To facilitate the computations we approximate both the emissivity of the four components and the dust opacity by exponentials of the form $C\exp\{-cD_G\}$, where C and c are for each component constants to be determined from observations. Exponentials and inner cut-offs of the distribution are listed in Table A1.

For the following analytical computations it is found useful to introduce the relations:

For the dust opacity and optical depth, respectively, we use

$$\begin{aligned} k &= k(0)\exp\{-\beta D_G\} \text{ with } k(0) = k_\odot \exp\{\beta D_\odot\} \\ \tau &= \tau(0)\exp\{-\beta D_G\} \text{ with } \tau(0) = \tau_\odot \exp\{\beta D_\odot\}. \end{aligned} \qquad \text{(A5a)}$$

For the emissivity of component ℓ

$$j_\ell(D_G) = j_\ell(0)\exp\{-\alpha_\ell D_G\} \quad \text{with} \quad j_\ell(0) = j_\ell^\odot \exp\{\alpha_\ell D_\odot\} \qquad \text{(A5b)}$$

Here, as usual, the symbol $\odot$ refers to the solar neighborhood and hence $D_\odot = 10$ kpc. Of course $j(0)$ and $k(0)$ are simply formal parameters for those distributions with an inner cut-off.

At any galactocentric distance D_G the mean intensity contributed by each component ℓ at the wavelength λ, $4\pi J_\lambda^\ell(D_G)$, is obtained from an integral similar to Eq. (A1). For the evaluation of these integrals we assume, similarily as for the evaluation of Eq. (A1), a latitude distribution $\propto 1 - e^{-\tau/\mu}$, with $\mu = \sin b$, independent

Table A1

Component ℓ	T_ℓ / K	W_ℓ	Inner cut-off $D_{\min,\ell}$ of distribution	Exponents α_ℓ, β	$\delta_\ell = \frac{\alpha_\ell - \beta}{\beta}$	Notes
1. Early type stars	(see text)		4	α_1 = 0.40	0.54	(a)
2. Disk stars	7500	1.0 E-14	0	α_2 = 0.25	-0.04	(b)
3. Disk stars	4000	1.0 E-13	0	α_3 = 0.25	-0.04	(b)
4. Red Giants	3000	4.0 E-13	4	α_4 = 0.75	1.88	(c)
Dust (i.e. opacity k and optical depth τ perpendicular to galactic plane)			4	β = 0.26	-	(d)
			0	(see footnote)	-	(e)

Notes:

a) $\alpha_1 = 0.40$ is a compromise between the gradient derived for the Lyc production rate of compact HII regions and of ELD HII regions (Mezger, 1978).

b) α_2, α_3 are derived from the observed surface brightness of spiral galaxies (Freeman, 1970) corrected for dust absorption with $\tau_V^\odot$ and β as used in this paper.

c) Derived from a fit to the observed 2.4 μm ridge line intensity given in Hayakawa et al. (1978) and the dust opacity used in this paper.

d) β = 0.26 has been estimated by Güsten (1981) between D_G = 5 and 12 kpc.

e) From D_G = 4–∿0 kpc we adopt a linear decrease of the visual extinction from 3.0 to 0 mag kpc^{-1} in accordance with Güsten (1981).

Table A2. Stellar emissivities in erg cm^{-2} s^{-1} μm^{-1} kpc^{-1} ster^{-1}

λ (μm)	10^3 $j_{O,1}$	10^3 $j_{O,2}$	10^3 $j_{O,3}$	10^3 $j_{O,4}$	λ (μm)	10^3 $j_{O,1}$	10^3 $j_{O,2}$	10^3 $j_{O,3}$	10^3 $j_{O,4}$
0.091	276	0.010	—	—	0.55	—	24.1	11.1	559
0.100	330	0.035	—	—	0.70	—	15.5	13.3	1023
0.110	402	0.110	—	—	0.90	—	8.43	11.7	1145
0.130	358	0.620	—	—	1.2	—	3.52	7.31	904
0.143	303	1.41	—	—	1.8	—	0.880	2.62	416
0.180	162	6.36	0.006	0.004	2.2	—	0.418	1.41	248
0.200	112	11.1	0.025	0.036	2.4	—	0.299	1.05	194
0.210	90.8	14.2	0.048	0.093	3.4	—	0.090	0.364	76.7
0.216	76.5	16.1	0.068	0.154	4.0	—	0.058	0.247	53.8
0.230	38.6	18.1	0.123	0.384	5.0	—	0.029	0.127	28.7
0.250	—	21.8	0.264	1.24	6.0	—	0.017	0.077	17.8
0.346	—	31.3	2.43	36.8	8.0	—	0.006	0.031	7.3
0.435	—	30.8	6.43	194					

of the galactic longitude l and an exponential dependence of the ridge line intensity on l

$$I(l)=I_c e^{-\gamma l}$$

with (A6)

$$\gamma=\pi^{-1}\ln(I_c/I_{ac}).$$

Hence, c and ac refer to the directions toward the galactic center ($l=0°$) and the anticenter ($l=180°$), respectively. Equation (A6) appears to be a reasonable approximation of the ridge line intensities for wavelengths $\lambda \lesssim 1$ μm, where, for example, at $D_G=10$ kpc, the dependence on longitude is small, $I_c/I_{ac}<4$. In the NIR, where the Galaxy becomes more and more transparent, Eq. (A6) is, of course, only a crude approximation of the ridge line intensities, such as, e.g. $I_{2.4}(l, b=0°)$ derived by Hayakawa et al. (1978). The integral for the mean intensity for component ℓ can be written in the form

$$4\pi J_\lambda^\ell(D_G)=2\int_0^\pi I_c^\ell e^{-\gamma l}dl\cdot 2\int_0^1(1-e^{-\tau/\mu})d\mu$$
$$=\phi_\lambda^\ell(D_G)\cdot F\{\tau_\lambda(D_G)\}, \quad \text{(A7a)}$$

$$\phi_\lambda^\ell(D_G)=2\int_0^\pi I_c^\ell e^{-\gamma l}dl=2\pi I_c^\ell\frac{(1-I_{ac}^\ell/I_c^\ell)}{\mathrm{en}(I_c^\ell/I_{ac}^\ell)}, \quad \text{(A7b)}$$

and

$$F\{\tau_\lambda(D_G)\}=2\int_0^1(1-e^{-\tau/\mu})d\mu=2[1-e^{-\tau}+\tau E_1(\tau)]. \quad \text{(A7c)}$$

It remains to express Eq. (A7b) in terms of $k(0)$ and $j_\ell(0)$ as defined by Eqs. (A5). This yields

$$I_{ac}^\ell(D_G)=\int_{D_G}^\infty j_\ell(r)\exp\left\{-\int_{D_c}^r kds\right\}dr$$
$$=A_\ell e^{-x}\int_0^x y^{\delta_\ell}e^y dy \quad \text{(A8a)}$$

with

$$x=\int_{D_G}^\infty k(0)e^{-\beta r}dr=\frac{k(0)}{\beta}e^{-\beta D_G}$$

$$A_\ell=\frac{j_\ell(0)}{k(0)}\left(\frac{\beta}{k(0)}\right)^{\delta_\ell} \quad \text{and} \quad \delta_\ell=\frac{\alpha_\ell-\beta}{\beta}.$$

The corresponding integral for I_c^l,

$$I_c^\ell(D_G)=\int_{D_{\min}}^{D_G} j_\ell(r)\exp\left\{-\int_r^{D_G} kds\right\}dr$$
$$+\exp\left\{-\int_{D_{\min}}^{D_G} kds\right\}\cdot\int_{D_{\min}}^\infty j_\ell(r)\exp\left\{-\int_{D_{\min}}^r kds\right\}dr \quad \text{(A8b)}$$

is valid for stellar components $\ell=1$ and 4 which have an inner cut-off at $D_G=D_{\min}$, which we assume to be the same as that of dust absorption. The first term represents the contribution from emission between $D_{\min}$ and D_G, while the second term represents emission coming from the opposite side of the galactic center.

The stellar components $\ell=2$ and 3 do not have an inner cut-off at 4 kpc. We therefore must add to the above expression for I_c^ℓ another term, ΔI_c^ℓ, which accounts for stellar emission between $0\leqq r\leqq D_{\min}$, where the density of disk stars still increases exponentially, while the dust opacity is lower than at 4 kpc and increases linearly with radius. For this additional term we can write the expression

$$\Delta I_c^\ell(D_G)=\exp\left\{-\int_{D_{\min}}^{D_G} kds\right\}\left[\int_0^{D_{\min}} j_\ell(r)\right.$$
$$\cdot\exp\left\{-\int_r^{D_{\min}} kds\right\}dr+\int_0^{D_{\min}} j_\ell(r)$$
$$\left.\cdot\exp\left\{-\int_0^{D_{\min}} kds-\int_0^w kds\right\}\right]dr \quad \text{(A8c)}$$

which is valid for $D_G\geqq D_{\min}$. We evaluate the integrals numerically, assuming that dust extinction k increases linearly with r for $r<D_{\min}$, and that there are 6 mag of visual extinction at r between

the center and $D_{min}=4$ kpc. This implies a visual extinction of 3 mag kpc^{-1} at $r=4$ kpc, which is consistent with Güsten's (1981) model.

The approximations used here are adequate for the purpose of estimating variations of the stellar ISRF relative to ISRF in the solar vicinity, which is based on direct observations, as discussed in Appendix C of Paper I and in the first section of this appendix. As for the dust opacity k_λ and optical depth τ_λ, respectively, all equations in this appendix are meant to include absorption only but not scattering. The relative opacities $k_\lambda/k_{0.55}$ and $\tau_\lambda/\tau_{0.55}$ (with 0.55 μm referring to the visual band) are given in Appendix C.

Equations (A7) and (A8) are numerically evaluated. The resulting average radiation intensity, $4\pi J_\lambda(D_G)$, is given for some selected galactocentric distances in Table A3. For $D_G=10$ and 5 kpc the total average radiation intensity as well as the individual contributions of the four components are shown in Fig. 1. In Fig. 2a is shown the variation of the integrated mean radiation intensity relative to the solar vicinity of both the total ISRF due to direct stellar radiation, $R_{st}(D_G)$, and for the individual four components, $R^\ell_{st}(D_G)$, with $\ell=1,2,3,4$.

New results, which combine 2.4 μm surveys of both the northern and southern sky were published by Hayakawa et al. (1981), after our model fits and computations of the ISRF were already completed. Compared with these new results, our model fit with $\alpha_4=0.75$, $W_4=4\,10^{-13}$ yields ridge line intensities, which for $l\lesssim 30°$ on the average are about 30% too high. With $\alpha_4=0.90$, $W_4=2.5\,10^{-13}$ we get a better fit of the ridge line intensities published by Hayakawa et al. (1981). This choice of W_4 would decrease the integrated intensity of the ISRF given by Eq. (A4) by 12%. However, the effect of these changes on the grain temperatures is negligible. Also note that Hayakawa et al. (1981) in interpreting their observations use a different extinction model, which corresponds to a visual extinction $A_V\sim 20$ mag between the sun and the galactic center, while our extinction model yields $A_V\sim 25.3$ mag.

Table A3. The ISRF between 0.09 and 8 μm at selected galactocentric distances D_G

$4\pi J_\lambda(D_G)$ in erg cm^{-2} s^{-1} μm^{-1}

D_G/Kpc / λ/μm	5	6	8	10	13
.091	3.01E-2	2.52E-2	1.70E-2	1.07E-2	4.85E-3
.10	4.43E-2	3.67E-2	2.40E-2	1.47E-2	6.45E-3
.11	6.56E-2	5.36E-2	3.40E-2	2.04E-2	8.54E-3
.13	6.99E-2	5.64E-2	3.48E-2	2.05E-2	8.48E-3
.143	6.40E-2	5.12E-2	3.14E-2	1.82E-2	7.46E-3
.18	4.27E-2	3.42E-2	2.10E-2	1.24E-2	5.16E-3
.20	3.22E-2	2.62E-2	1.68E-2	1.04E-2	4.71E-3
.21	2.74E-2	2.26E-2	1.50E-2	9.61E-2	4.68E-3
.216	2.47E-2	2.06E-2	1.40E-2	9.17E-3	4.63E-3
.230	2.05E-2	1.73E-2	1.21E-2	8.25E-3	4.26E-3
.250	1.41E-2	1.26E-2	9.79E-3	7.27E-3	4.04E-3
.346	3.67E-2	2.79E-2	1.97E-2	1.30E-2	6.29E-3
.435	5.36E-2	3.90E-2	2.40E-2	1.50E-2	7.01E-3
.55	8.28E-2	5.49E-2	2.82E-2	1.57E-2	6.85E-3
.70	1.15E-1	7.14E-2	3.10E-2	1.53E-2	5.98E-3
.90	1.20E-1	7.77E-2	2.97E-2	1.32E-2	4.70E-3
1.20	9.35E-2	5.79E-2	2.18E-2	9.26E-3	3.11E-3
1.8	3.88E-2	2.48E-2	9.60E-3	4.06E-3	1.33E-3
2.2	2.18E-2	1.41E-2	5.61E-3	2.41E-3	8.02E-4
2.4	1.62E-2	1.06E-2	4.31E-3	1.89E-3	6.38E-4
3.4	4.75E-3	3.18E-3	1.39E-3	6.49E-3	2.32E-4
4.0	2.62E-3	1.77E-3	7.96E-4	3.79E-4	1.39E-4
5.0	1.20E-3	8.09E-4	3.67E-4	1.76E-4	6.48E-5
6.0	6.15E-4	4.17E-4	1.91E-4	9.21E-5	3.41E-5
8.0	2.13E-4	1.45E-5	6.65E-5	3.22E-5	1.19E-5

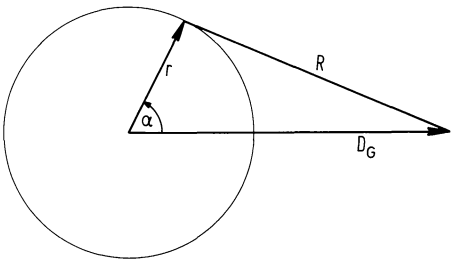

Fig. B1. Geometry for model computations of the intensity of the FIR part of the ISRF. D_G is the galactocentric distance

Appendix B: the ISRF from λ8 μm to λ1000 μm

The spectrum of the ISRF at $l\sim 30°$, $b\sim 0°$ in this wavelength range and for the solar vicinity is given in Fig. 3 of Paper I, keeping in mind that the points labelled "Pr" must be decreased by a factor of 0.7 (see "note added in proof" Paper I). To evaluate the integral $\int_{4\pi} I_\lambda(l,b)d\Omega$ we assume a gaussian distribution of HPW θ_b in latitude and we adopt for the longitudinal distribution the ridge line intensity measured by Boissé et al. (1981) in the wavelength band 114–196 μm. Since the ridge line intensity is very much smaller at $l\approx 90°$ than for $l<60°$, we neglect the contribution of $l>90°$. Then

$$\int_{4\pi} I_\lambda(l,b)d\Omega = I_\lambda(l=30°,b=0°)2\int_0^{90°}\frac{I_{114-196}(l)}{I_{114-196}(l=30°)}dl \cdot \int_{-\pi/2}^{+\pi/2}\exp\{-b^2/(0.6\theta_b)^2\}\cos b db$$

with

$$\int_0^{90°}\ldots dl = 45.^\circ 7 \quad \text{and} \quad \int_{-\pi/2}^{+\pi/2}\exp\{\ldots\}\cos b db \simeq 1.06\Theta_b .$$

From Nishimura et al. (1980) we take $\theta_b\simeq 1.7°$ and obtain

$$4\pi J_\lambda^\odot = I_\lambda(l=30°,b=0°)\Omega_\odot \qquad \text{(B1)}$$

with $\Omega_\odot=5.0\ 10^{-2}$ sr. The corresponding values for $8\leqq\lambda/\mu m\leqq 1000$ are given in Table B1.

For a computation of $4\pi J_\lambda(D_G)$ for galactocentric distances $2.5\leqq D_G/\text{kpc}\leqq 11.5$ we assume the Galaxy to be optically thin for $\lambda\geqq 10$ μm. Therefore, the intensity is solely determined by the product of the emissivity times the geometric dilution factor integrated over the volume. Our model consists of concentric rings of width $\Delta r=1$ kpc and height $h=117$ pc (Boissé et al., 1981). The geometry is shown in Fig. B1. D_G is the galactocentric distance for which $4\pi J(D_G)$ shall be computed. The calculations are made adopting the behaviour of the volume emissivity $j(D_G)$ as derived by Boissé et al. (1981). The volume element $r d\alpha \Delta r h$ contributes to $4\pi J(D_G)$ the intensity $r d\alpha \Delta r h\varepsilon(r)/4\pi R^2$, and the total ring contributes the intensity

$$4\pi J(r,D_G) = r\Delta r h 2\int_0^\pi \frac{j(r)\,dr}{4\pi(D_G^2+r^2-2rD_G\cos\alpha)}.$$

Table B1. The ISRF between 8 and 1000 μm in the solar vicinity ($D_G = 10$ kpc)

λ	$4\pi J_\lambda^\odot$	λ	$4\pi J_\lambda^\odot$	λ	$4\pi J_\lambda^\odot$	λ	$4\pi J_\lambda^\odot$
8	4.33 E-5	30	1.70 E-5	80	4.20 E-5	300	1.39 E-6
10	3.26 E-5	40	3.06 E-5	90	3.62 E-5	400	5.61 E-7
12	2.21 E-5	50	4.08 E-5	100	3.16 E-5	600	1.32 E-7
20	7.13 E-6	60	4.76 E-5	150	1.36 E-5	800	4.20 E-8
25	1.14 E-5	70	4.51 E-5	200	5.61 E-6	1000	2.14 E-8

λ is in μm, $4\pi J_\lambda^\odot$ in erg cm^{-2} s^{-1} μm^{-1}
To compute $4\pi J_\lambda^\odot(D_G)$ use eq. (7) with R_{Dust} from Fig. 2b

Solving the integral we obtain

$$4\pi J(r, D_G) = \frac{1}{2} \frac{r \Delta r h j(r)}{|D_G^2 - r^2|}. \tag{B2}$$

This result is valid for $D_G - r \gg h$. The quantity $4\pi J_\lambda(D_G)$ is obtained by summing over all rings. For $r = D_G > 12$ kpc we put $\varepsilon(r) = 0$ because the observations by Boissé et al. strongly suggest that the contribution beyond $D_G > 12$ kpc is negligibly small. Evaluating the average intensity integrated over solid angle with the Boissé et al. emissivity we obtain

$$4\pi J(D_G = 10\,\text{kpc}) = 8.8\ 10^{-3}\ \text{erg cm}^{-2}\,\text{s}^{-1}.$$

However, the corresponding integral in Table B1 yields a value which is by about a factor 1.77 lower, i.e. $4\pi J^\odot = 5.0\ 10^{-3}$ erg cm^{-2} s^{-1}. This difference is due to the fact that the spectra used by Boissé et al. [shown as curve (PS) in Fig. 3 of Paper I] is considerably higher over the interval $2\,\mu\text{m} < \lambda < 50\,\mu\text{m}$ from what we consider to be the best fit to the spectrum of the diffuse galactic IR emission. This best fit is based on the observations by Price (1981), decreased by a factor of 0.7 over those plotted in Paper I. Furthermore, Boissé et al. apparently integrate over both stellar and dust component of the ISRF to estimate a bolometric correction while we, like Price (1981), conclude that the dust radiation dominates only for $\gtrsim 8$ μm.

While this difference in the integrated spectra will affect the total IR luminosity, it will not, however, affect relative values of $4\pi J(D_G)$. We therefore use the relation

$$4\pi J_\lambda(D_G) = 4\pi J_\lambda^\odot \frac{\sum_r 4\pi J(D_G, r)}{\sum_r 4\pi J(D_G = 10\,\text{kpc}, r)} = 4\pi J_\lambda^\odot R_{\text{Dust}}(D_G) \tag{B3}$$

for the computation of $4\pi J_\lambda(D_G)$. The values of $4\pi J_\lambda^\odot$ are those given in Table B1, the quantity $4\pi J(D_G, r)$ is given by Eq. (B2), and $\varepsilon(r)$ is taken from Fig. 3 of Boissé et al. The quantity

$$R_{\text{Dust}}(D_G) = \frac{\sum_r 4\pi J(D_G, r)}{\sum_r 4\pi J(D_\odot, r)} \tag{B4}$$

is shown in Fig. 2b. Together with Table B1 this allows to compute the ISRF due to reemission of stellar radiation absorbed by dust grains for any given galactocentric distance D_G between 4 and 13 kpc.

Appendix C: the dust model

Only a limited number of observations exist for the extinction $A(\lambda)$ for dust within even the outer layers of dark clouds. For the diffuse interstellar medium, $A(\lambda)$ is well determined. In the visual spectral region, $a(\lambda)$ and $g(\lambda)$ are rather high; there is great uncertainty about both parameters in the ultraviolet (Savage and Mathis, 1979; Paresce and Jakobsen, 1980). In this paper, we adopt the $A(\lambda)$ to be the *observed* relation as tabulated by Savage and Mathis (1979). To estimate $g(\lambda)$ and $a(\lambda)$, and to divide the observed extinction between grain components, a theoretical model of the grains is used. The grains are assumed to be the mixture of uncoated silicate and graphite particles suggested by (MRN), in which both silicates and graphite have a power-law size distribution with $n(a)$, the number density of particles between a and $a + da$ in size, being proportional to $a^{-3.5}\,da$. All of the silicon is assumed to be in silicates, and 0.8 of the carbon in graphite, with solar abundances. Each distribution is truncated at 0.01 μm for small sizes and 0.25 μm for large sizes. Under these conditions, there is very good agreement with the observed $A(\lambda)$. This model is used to assign each material its fraction of the extinction cross-section. Also, the $a(\lambda)$ and $g(\lambda)$ can be computed for each material by standard Mie theory, and the averaged $a(\lambda)$ and $g(\lambda)$ found by summing the component cross-sections straight forwardly.

It is easy to obtain the extinction cross-section per H atom in the solar neighborhood, $\sigma_\lambda^H(D_\odot)$, by the relation between H column density and $E(B-V)$ (Bohlin et al., 1978), plus the standard relation $A_V = 3.1\ E(B-V)$.

Table C1 tabulates the observed extinction cross-sections, relative to the V band (0.55 μm), and the theoretically derived extinction of each component, as well as $a(\lambda)$ and $g(\lambda)$. The footnote gives the conversion factor to (cm^2/H atom) in the solar neighborhood.

There is one ambiguity in silicate cross-sections which cannot be easily resolved. For pure minerals, silicates are almost perfect dielectrics and act only as scatterers. Realistically, there must be impurities which produce some absorption. In the present calculation, the index of refraction for silicates has been taken to be $(1.6 - 0.01i)$ in the visual wavelength region, which is reasonable in view of the fact that Martin and Angel (1977) have shown that the particles responsible for the interstellar polarization are also very good dielectrics (we estimate $k \lesssim 0.02$ if $n \simeq 1.5$). These polarizing particles are widely assumed to be silicates because of the polarization of the 9.7 μm silicate feature in some objects. However, the silicate absorption in the visual could well be somewhat higher than assumed here, but not enough to dominate graphite.

Observations show that dust in dark clouds has larger values of $R \equiv A_V/(A_B - A_V)$, and also of $\lambda_{\max}$, the wavelength of maximum linear polarization, than does dust in the diffuse interstellar medium. Both observations are usually interpreted as indicating larger particle sizes within clouds, although Chini and Krügel (1982) have shown that large R and $\lambda_{\max}$ can be produced by size distribution with a "normal" mean size. We feel that the MRN model which applies to dust in the diffuse ISM and probably represents the cores in a core-mantle dust model is appropriate for our calculations, because most of the absorption of the incident ISRF occurs in a layer which is optically thick in the ultraviolet but of modest opacity in the visual. Furthermore, Mathis and Wallenhorst (1981) have shown that the excitation of stars in dark clouds can be quantitatively understood with a normal graphite distribution (which provides most of the absorption in the visual)

Table C1. Assumed dust properties[1]

	Mixture			Graphite			Silicate		
λ(μm)	$A(\lambda)/A_V$	a(λ)	g(λ)	$A(\lambda)/A_V$	a(λ)	g(λ)	$A(\lambda)/A_V$	a(λ)	g(λ)
0.091	5.72	0.42	0.60	2.54	0.45	0.56	3.18	0.39	0.64
.10	4.65	.43	.59	2.11	.48	.55	2.54	.40	.63
.13	2.96	.45	.61	1.14	.52	.63	1.82	.40	.60
.143	2.70	.45	.63	.92	.52	.69	1.77	.41	.59
.18	2.49	.53	.58	1.07	.36	.62	1.42	.65	.57
.20	2.78	.56	.54	1.50	.36	.53	1.28	.79	.54
.21	3.00	.56	.51	1.76	.38	.46	1.24	.81	.55
.216	3.12	.56	.49	1.92	.40	.42	1.20	.83	.55
.23	2.86	.63	.48	1.80	.50	.39	1.06	.86	.57
.25	2.35	.63	.49	1.40	.47	.39	.95	.87	.57
.346	1.58	.71	.52	.87	.51	.46	.71	.95	.56
.435	1.32	.67	.52	.75	.46	.44	.57	.95	.57
.55	1.00	.63	.49	.62	.43	.39	.38	.95	.56
.7	.75	.56	.40	.52	.40	.31	.23	.93	.48
.9	.48	.50	.32	.37	.37	.24	.11	.91	.42
1.2	.280	.37	.12	.237	.28	.06	.042	.85	.23
1.8	.160	.25	.03	.147	.21	.01	.0135	.68	.10
2.2	.122	.22	.013	.113	.19	.0	8.6(-3)	.57	.12
2.4	.093	.15	.015	.087	.12	.0	6.5(-3)	.52	.06
3.4	.038	.058	.006	.036	.05	.0	2.6(-3)	.17	.03
4	.024	.046	.0	.022	.05	.0	2.0(-3)	.0	.0
5	.018	.0	.0	.015	.0	.0	2.7(-3)	.0	.0
6	.014	.0	.0	.010	.0	.0	3.4(-3)	.0	.0
8	.013	.0	.0	5.5(-3)	.0	.0	5.3(-3)	.0	.0
10	.072	.0	.0	3.9(-3)	.0	.0	6.8(-2)	.0	.0
12	.030	.0	.0	2.9(-3)	.0	.0	2.7(-2)	.0	.0
20	.065	.0	.0	2.3(-3)	.0	.0	6.3(-2)	.0	.0
25	.062	.0	.0	2.6(-3)	.0	.0	5.9(-2)	.0	.0
30	.032	.0	.0	3.5(-3)	.0	.0	2.9(-2)	.0	.0
40	.017	.0	.0	3.2(-3)	.0	.0	1.4(-2)	.0	.0
50	.014	.0	.0	2.5(-3)	.0	.0	1.2(-2)	.0	.0
60	.012	.0	.0	1.9(-3)	.0	.0	9.8(-3)	.0	.0
70	9.7(-3)	.0	.0	1.4(-3)	.0	.0	8.3(-3)	.0	.0
80	8.5(-3)	.0	.0	1.1(-3)	.0	.0	7.4(-3)	.0	.0
100	6.5(-3)	.0	.0	6.8(-4)	.0	.0	5.8(-3)	.0	.0
150	3.7(-3)	.0	.0	2.9(-4)	.0	.0	3.4(-3)	.0	.0
200	2.5(-3)	.0	.0	1.6(-4)	.0	.0	2.3(-3)	.0	.0
300	1.1(-3)	.0	.0	4.8(-5)	.0	.0	1.1(-3)	.0	.0
400	6.7(-4)	.0	.0	3.7(-5)	.0	.0	6.3(-4)	.0	.0
600	2.5(-4)	.0	.0	1.4(-5)	.0	.0	2.4(-4)	.0	.0
800	1.4(-4)	.0	.0	7.7(-6)	.0	.0	1.3(-4)	.0	.0
1000	7.3(-5)	.0	.0	4.8(-6)	.0	.0	6.8(-5)	.0	.0

(1) A(λ) = extinction, relative to the total extinction of the mixture at 0.55 μm. For extinction per H atom near the Sun, multiply by 5.34(-22) cm^2 (H atom)$^{-1}$.
a(λ) = albedo; g(λ) = <cos θ> = average cosine of angle of scattering.

and a larger-than-normal silicate distribution (which provides visual extinction through scattering, and therefore does not reduce the radiation field in the cloud significantly). Coatings are also apparently not the cause of the abnormal extinction, since ϱOph, the star lying deepest in a cloud for which the total hydrogen column density is known, has the *smallest* extinction per H known (Bohlin et al., 1978), as one would expect for grain coalescence. Condensing a mantle onto the grain would, of course, produce a *larger* extinction per H atom. Furthermore, HD 147889, a star behind ~5 mag visiual extinction in the ϱOph cloud, shows a large R, (~4.2), but no trace of the 3.1 μm "ice" band at even the 1–2% level (McMillan, 1978).

Presumably, at some large value of A_V within the cloud there are icy mantles formed on the grains, since at about $A_V=25$ mag the 3.1 μm ice band appears (Harris et al., 1978). In this paper, the grains' optical properties are not changed even then. For one thing, at that optical depth the radiation field in the visual is so low that the visual grain properties have little influence on any heating. However, the effects of mantles on FIR absorption are probably substantial, and our derived grain temperatures for $A_V>25$ must be considered quite provisional. Until more is known regarding the nature of the mantles, it is not even clear whether the coated grains should be warmer or colder than uncoated ones are calculated to be.

For predicting the ISRF at locations in the Galaxy we need not the dust absorption per H atom, but rather the mean extinction per kpc. We assume the wavelength dependence of all dust properties is the same as our estimate for the local values, given in Table C1. We define an opacity exponent β by writing the absorption coefficient (optical depth per kpc) proportional to $\exp(-\beta D_G)$. The absolute value of the opacity is determined from the condition that the extinction from the 4 kpc ring to the sun is $A_v(4\text{–}10\,\text{kpc})=19.5$, adopting an exponent $\beta=0.26$ for the dust density distribution (Güsten, 1981) and an albedo at $\lambda=0.55$ μm of a (0.55 μm)=0.63 (MRN). This gives an absolute opacity at the solar circle of

$$k_{\text{abs}}^{\odot}(V)=0.460\,\text{kpc}^{-1}$$

and

$k_{ext}^{\odot}(V) = 1.23\,\mathrm{kpc}^{-1}$.

Also, assuming the scale height of dust to be the same as that of the diffuse atomic hydrogen, namely $h = 130$ pc (Burton et al., 1975), the absorption optical depth perpendicular to the galactic plane is $\tau_V^{\odot} = 0.060$, which implies an extinction $A_V = 0.17$ mag perpendicular to the plane.

The grain model here represents one extreme of separation of the two materials. It is entirely possible, or even likely, that small particles of materials other than graphite are found in the "graphite" particles, and likewise for silicates. The reason why pure graphite particles attain such high temperatures is that graphite has a low absorption coefficient in the FIR; adding even a little material of very large opacity to a graphite grain would allow it to cool a significant amount. Mixing the types of particles would have much less effect on the extinction of the mixture, from which the composition was derived.

Observations of the width of the FIR emission from isolated dark clouds should provide an observational test to determine the temperature of the graphite grains. On the other hand, the circular polarization shows that graphite is not strongly mixed with the grains which provide the polarization (silicates, on our model), so at present it is reasonable to assume the substances are in fact separated into two groups of particles.

Besides knowing what the absorption properties of grains are, we must consider the variation of opacity within the Galaxy. As Eq. (1) shows, the opacity exponent β is determined by absorption in both the H I gas and in H_2 clouds (observed though their CO emission). Much of this H_2 material is probably in clouds which are rather transparent at $\lambda \approx 1$ μm.

Bohlin et al. (1978) found that H_2 absorption seen against stars becomes appreciable rather abruptly when $E(B-V) \approx 0.2$, or $A_V \approx 0.6$. The dust associated with this rather diffuse H_2 will affect the entire ISRF, since such matter is rather widespread. On the other hand, the dust associated with the H_2 in GMC's does not greatly affect the ISRF per H_2 molecule because the GMC's occupy a very small angle in the sky, and most of their dust absorbs little energy because it is in the dark cloud. The value $\beta = 0.26\,\mathrm{kpc}^{-1}$ is the average opacity exponent for a line drawn from the sun into the inner regions of the Galaxy, including the opacity in the interiors of any dark clouds along the way (Güsten, 1981). Probably the opacity in the H_2 zones should not be counted at all for the far-ultraviolet wavelengths, since H_2 cannot exist where such radiation is strong. On the other hand, it takes a rather opaque cloud to absorb much $\lambda > 2$ μm radiation, and most of the opacity associated with small H_2 clouds should be used for these longer wavelengths. A minimum value of β, ignoring all absorption in H_2 gas completely, is set by the gradient in heavy elements. Güsten (1981) suggests the composition varies by about a factor of 2 in heavy elements (and hence dust opacity per H atom) between the sun and $D_G = 4$ kpc. This corresponds to $\exp[-0.12(D - D_{\odot})]$, so $\beta = 0.12$ is a lower limit. To test the sensitivity of our results to β we also computed models with values of $\beta = 0.20\,\mathrm{kpc}^{-1}$ and $0.12\,\mathrm{kpc}^{-1}$, respectively, instead of the standard $0.26\,\mathrm{kpc}^{-1}$. These models give virtually identical results to the standard one in every respect, primarily because the total extinction between the Sun and the Galactic center is fixed at 25.5 mag at V. This constraint serves to fix the characteristics of the model. Thus we are not concerned about the precise value of β which is in fact appropriate.

References

Bohlin, R.C., Savage, B.D., Drake, J.F.: 1978, *Astrophys. J.* **224**, 132

Boissé, P., Gispert, R., Coron, N., Wijnbergen, J., Serra, G., Ryter, C., Puget, J.L.: 1981, *Astron. Astrophys.* **94**, 265

Bollea, D., Cavaliere, A.: 1976, *Astron. Astrophys.* **49**, 313

Burton, W.B., Gordon, M.A., Bania, T.M., Lockmann, F.J.: 1975, *Astrophys. J.* **202**, 30

Chini, R., Krügel, E.: 1981, *Astron. Astrophys.* (in press)

Code, A.D.: 1973, *Proc.* IAU *Symp.* **52**, eds. J.M. Greenberg and H.C. van de Hulst, p. 505

Flannery, B.P., Roberge, W., Rybicki, G.B.: 1980, *Astrophys. J.* **236**, 598

Freeman, K.C.: 1970, *Astrophys. J.* **160**, 811

Guiderdoni, B., Rocca-Volmerange, B.: 1982, *Astron. Astrophys.* **109**, 355

Güsten, R.: 1981, unpublished thesis, Univ. of Bonn (see also Güsten, R., Mezger, P.G., review paper, Vistas in Astronomy (in press)

Harris, D.H., Woolf, N.J., Rieke, G.H.: 1978, *Astrophys. J.* **226**, 829

Hayakawa, S., Ito, K., Matsumoto, T., Uyama, K.: 1977, *Astron. Astrophys.* **58**, 325

Hayakawa, S., Ito, K., Matsumoto, T., Murakami, H., Uyama, K.: 1978, *Publ. Astron. Soc. Japan* **30**, 369

Hayakawa, S., Matsumoto, T., Murakami, H., Uyama, K., Yamagami, T., Thomas, J.A.: 1979, *Nature* **279**, 510

Hayakawa, S., Matsumoto, T., Murakami, H., Uyama, K., Thomas, J.A., Yamagami, T.: 1981, *Astron. Astrophys.* **100**, 116

Jura, M.: 1979, *Astrophys. Letters* **20**, 89

Kawara, K., Kozasa, T., Sato, S., Kobayashi, Y., Okuda, H., Yugaku, J.: 1982, *Publ. Astron. Soc. Japan* **34**, 389

Keene, J.: 1981, *Astrophys. J.* **245**, 115

Maihara, T., Oda, N., Sugiyama, T., Okuda, H.: 1978, *Publ. Astron. Soc. Japan* **30**, 1

Martin, P.G., Angel, J.R.P.: 1977, *Astrophys. J.* **207**, 126

Mathis, J.S., Rumpl, W., Nordsiek, K.H.: 1977, *Astrophys. J.* **217**, 425 (MRN)

Mathis, J.S., Wallenhorst, S.: 1981, *Astrophys. J.* **244**, 483

McMillan, R.S.: 1978, *Astrophys. J.* **225**, 417

Mezger, P.G.: 1978, *Astron. Astrophys.* **70**, 565

Mezger, P.G.: 1983, Proc. of the XVI ESLAB Symp. Toledo, Spain (in press)

Mezger, P.G., Mathis, J.S., Panagia, N.: 1982, *Astron. Astrophys.* **105**, 372 (Paper I)

Natta, A., Palla, F., Panagia, N., Preite-Martinez, A.: 1981, *Astron. Astrophys.* **99**, 289

Okuda, H.: 1980, *Proc.* IAU *Symp.* **96**, eds. C.G. Wynn-Williams and D.P. Cruikshank, p. 247

Paresce, F., Jacobsen, P.: 1980, *Nature* **288**, 119

Price, S.D.: 1981, *Astron. J.* **86**, 193

Savage, B.D., Mathis, J.S.: 1979, *Ann. Rev. Astron. Astrophys.* **17**, 73

Serra, G., Puget, J.L., Ryter, C.E.: 1980, *Astron. Astrophys.* **84**, 220

Smith, J.: 1982, *Astrophys. J.* **261**, 463

Solomon, P.M., Sanders, D.B., Scoville, N.Z.: 1978, *Proc.* IAU *Symp.* **84**, ed. W.B. Burton, p. 35

Werner, M.W., Salpeter, E.E.: 1969, *Monthly Notices Roy. Astron. Soc.* **145**, 249

Werner, M.W., Salpeter, E.E.: 1970, Proc. 16th Liège Symp., Institut d'Astrophysique de l'Université de Liège, p. 113